THE DAVID W. TAYLOR MODEL BASIN

UNITED STATES NAVY

ANALYSIS OF TEST DATA ON THE PERFORMANCE CHARACTERISTICS OF PLANING AND DISPLACEMENT FLOATS FOR SUPPORTING SUBMERGED LOADS

P. EISENBERG

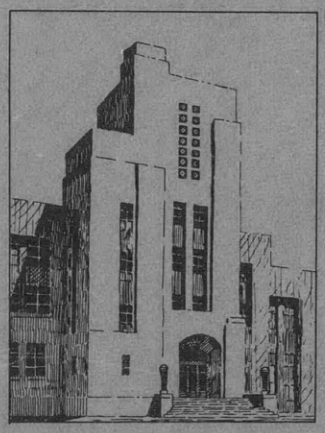

[redacted]

OCTOBER 1947

REPORT 573

PERSONNEL

The project was conducted under the management of P. Eisenberg, who prepared the TMB float designs for this application and carried out the model-basin tests and subsequent analyses. G. Grimminger, formerly of the Taylor Model Basin staff, designed the faired weights used in the experiments. L. Pode assisted in certain phases of data analysis. E. Larson carried out the measurements on the TMB planing float during the tests for structural failure.

The report was written by Mr. Eisenberg.

REPORT 573

ANALYSIS OF TEST DATA ON THE PERFORMANCE CHARACTERISTICS OF PLANING AND DISPLACEMENT FLOATS FOR SUPPORTING SUBMERGED LOADS

P. EISENBERG

OCTOBER 1947

TABLE OF CONTENTS

ANALYSIS OF TEST DATA ON THE PERFORMANCE CHARACTERISTICS OF PLANING AND DISPLACEMENT FLOATS FOR SUPPORTING SUBMERGED LOADS

ABSTRACT

Data on the performance characteristics of a planing float and of a displacement float, originally designed for supporting a catenary loop of minesweeping cable, are analyzed. The planing float was a prototype of the TMB planing float and was constructed of welded steel. The displacement float was in the form of a body of revolution and was constructed of balsa wood.

The data on the planing float in the planing regime are compiled into a single nondimensional relationship between drag, total load, and speed-length ratio. The characteristics of the balsa-wood displacement float are also presented in nondimensional form as a family of curves of drag coefficient plotted on speed-length ratio with a load coefficient as parameter.

A region of instability was shown to exist in the transition from subsurface to surface operation of the TMB planing float, and a hysteresis loop in the drag characteristics of this float was discovered. It was also found that this float, as well as the displacement float, exhibits the same type of striations in the flow over the float when towed near the water surface, just before complete emergence, as is shown by spheres and projectiles dropped through an air-water interface. A hypothesis based on the instability of the vortex formed near the point of separation is offered as a more adequate explanation of this phenomenon than the idea of cavitation formation about minute nuclei on or near the surface of the specimen.

A displacement float submitted by the Naval Mine Warfare Test Station was also tested, but no analysis of the data was made since the tests showed that the float was not useful for supporting submerged loads. The tests of the Naval Mine Warfare Test Station float are reported in an appendix. Observations of the performance of this float and of the TMB planing float towed in a seaway are discussed. Pressure tests to determine the maximum depth of submergence of the steel planing float before complete collapse, and problems in the construction and waterproofing of the balsa-wood float are also considered in appendixes.

INTRODUCTION

In November 1943 the David Taylor Model Basin was requested (1)* to undertake the design and development of floats for supporting submerged loads.

---

* Numbers in parentheses indicate references on page 44 of this report.

The immediate application accompanying this request required floats for supporting a towed cable which formed, approximately, a catenary loop when the ends were secured to two vessels towing abreast in minesweeping operations, as shown in Figure 1. Based on the specifications for the catenary-sweep problem, the first design was a steel float geometrically similar to the TMB

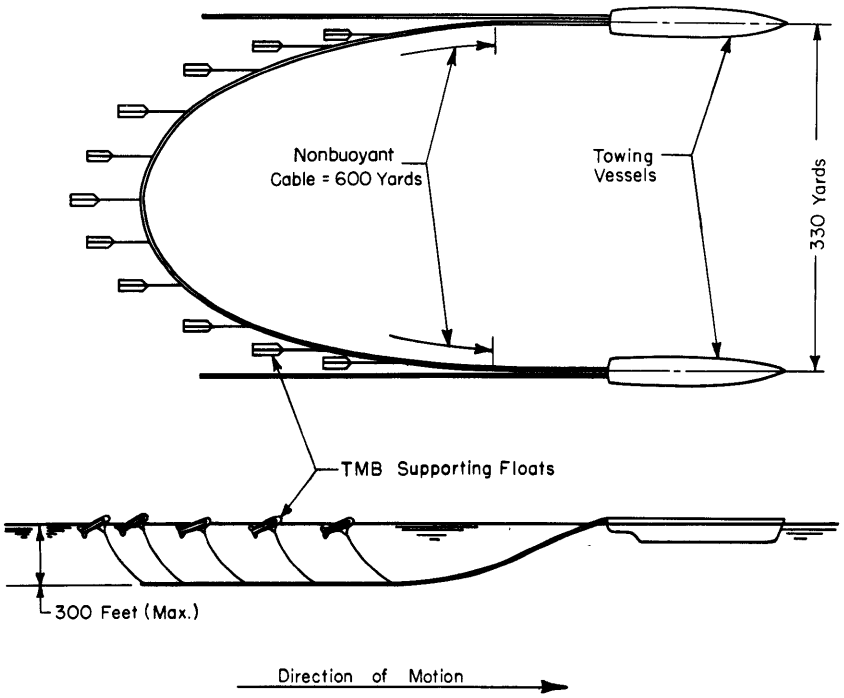

Figure 1 - Towing Arrangement for a Catenary-Type Minesweeping Arrangement

planing float which is used as an indicator of the position of underwater bodies (2). After this float was developed, the Taylor Model Basin was requested to investigate the possibilities of designing a displacement float with a hull of balsa wood (3). It was thought that such a float would develop ample buoyancy with a large saving in weight as compared with the metal planing float. In addition to these two floats, a third float submitted by the Naval Mine Warfare Test Station (NMWTS), Solomons, Maryland, was also tested for load-carrying applications. This float is of hollow, sheet-metal construction and consists simply of a cylindrical body with conical bow and stern.

Although initial tests to determine the hydrodynamic characteristics of these floats were primarily intended to check the practicability of the final designs, sufficient data were subsequently gathered to serve as a basis for a rather complete analysis of performance characteristics. The

data for the TMB floats have been reduced to nondimensional form so that they may be used in the selection of geometrically similar floats for any applications in which submerged loads must be towed from surface floats.

Since the characteristics of the TMB planing float under load in the displacement regime were already known (2), the tests were extended to determine its performance in the planing regime. For the range of Reynolds numbers over which this design is likely to be used, it was possible to compile the data in the planing regime into a single nondimensional relationship between drag, total load, and speed-length ratio. The characteristics of the balsa-wood float are also presented in nondimensional form as a family of curves of drag coefficient plotted against speed-length ratio, with a load coefficient as parameter. Since the performance of the NMWTS float indicated that this float is not useful for towing submerged loads, no analysis has been made for this float.

The tests disclosed phenomena in the region of transition from subsurface to surface operation of a symmetrical shape such as the TMB planing float, which it is believed have not been reported hitherto. A hysteresis loop in the drag characteristics of the float was also discovered in this unstable region. It was found that this float, as well as the balsa-wood displacement float, exhibits the same type of striations in the flow over the float when towed near the water surface, just before complete emergence, as is shown by spheres and projectiles dropped through an air-water interface. A hypothesis based on the instability of the vortex formed near the point of separation of flow is offered in explanation of the latter observation.

The particular sizes of floats used in the tests considered herein were determined on the basis of the catenary-sweep project. Since this project represents only one application of these floats, the results are analyzed in terms of the general problem. Accordingly, the overall considerations of hydrodynamic design and performance of the TMB floats are considered in the body of the report. The tests of the NMWTS float are discussed in Appendix 1. The applications to the catenary-sweep problem including observations of the floats during full-scale trials in a seaway are considered in Appendix 2. Problems of the structural design of the planing float as well as the results of submergence tests on this float to determine the maximum safe depth of submergence before failure are discussed in Appendix 3. Problems of construction and waterproofing of the balsa-wood float are considered in Appendix 4.

PERFORMANCE CHARACTERISTICS OF THE TMB PLANING FLOAT

It has been pointed out that the particular floats used in the experiments discussed herein were selected on the basis of the catenary-sweep

requirements. However, the design principles of the TMB planing float already had been developed when the catenary-sweep project was initiated. Furthermore, the analysis of experimental data in this report is applied only to the planing regime. To provide the necessary background on the development of this float, the principal features of the float, its characteristics in the displacement regime, and the design features as used for the catenary sweep will be discussed before proceeding with the present topics.

DESIGN OF THE TMB PLANING FLOAT

The TMB planing float has been completely described in Reference (2). It is symmetrical about a horizontal plane and about a longitudinal vertical plane. The bow is in the form of two elliptical cones which are faired into flat plates forming an angle of dead rise of 10 degrees. A sketch of the float in which the dimensions are referred to the beam *b* is shown in Figure 2. The float surfaces are completely developable, as shown

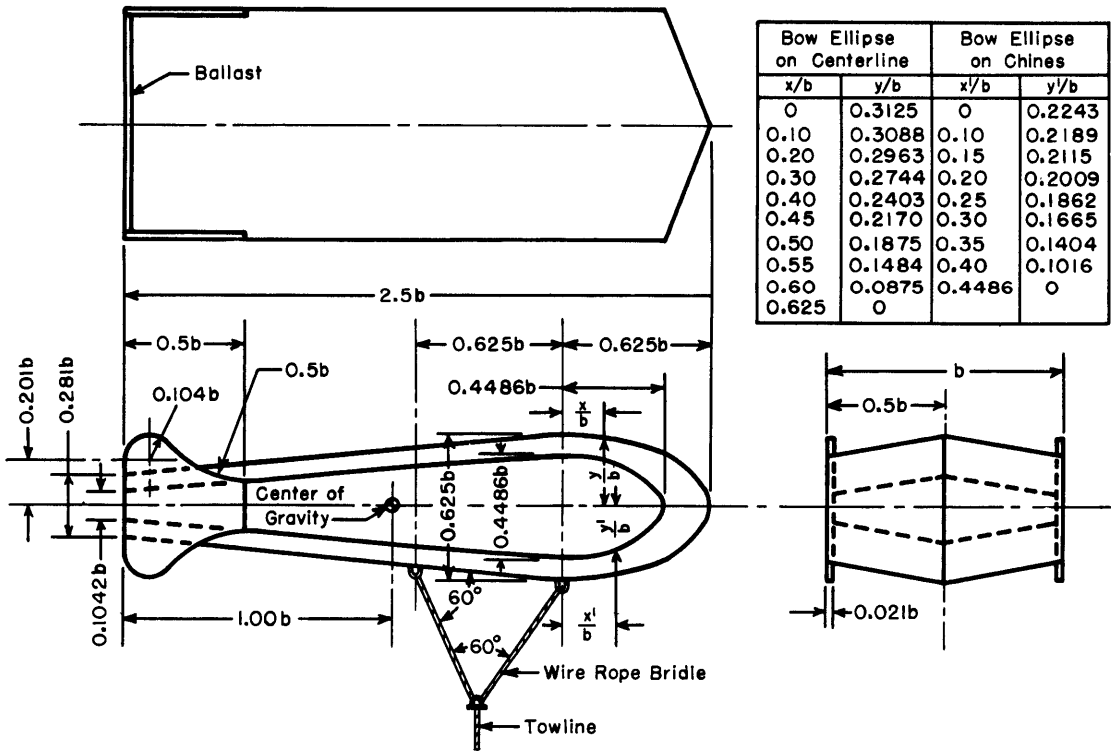

Bow Ellipse on Centerline		Bow Ellipse on Chines	
x/b	y/b	x'/b	y'/b
0	0.3125	0	0.2243
0.10	0.3088	0.10	0.2189
0.20	0.2963	0.15	0.2115
0.30	0.2744	0.20	0.2009
0.40	0.2403	0.25	0.1862
0.45	0.2170	0.30	0.1665
0.50	0.1875	0.35	0.1404
0.55	0.1484	0.40	0.1016
0.60	0.0875	0.4486	0
0.625	0		

Figure 2 - Dimensioned Sketch of TMB Planing Float

All dimensions are referred to a selected beam *b*.

in Figure 3; the analytical methods employed in arriving at the developable shape as well as a history of the development of the float are given in Reference (2). A photograph of a TMB planing float, 41 inches in length, is shown

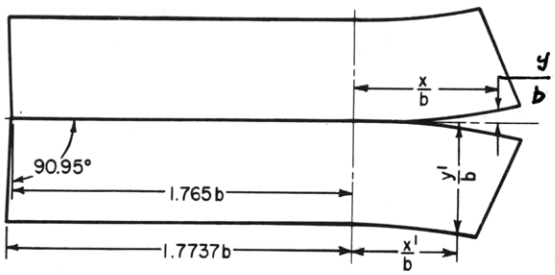

Developed Curve on Centerline		Developed Curve on Chines	
x/b	y_s/b	x'/b	y'/b
0	0	0	0.5082
0.1175	0.0009	0.1484	0.5082
0.1722	0.0021	0.1872	0.5104
0.2262	0.0035	0.2257	0.5118
0.2798	0.0054	0.2631	0.5134
0.3320	0.0076	0.3002	0.5151
0.3837	0.0100	0.3362	0.5176
0.4337	0.0135	0.3706	0.5200
0.4817	0.0170	0.4039	0.5229
0.5280	0.0209	0.4354	0.5260
0.5719	0.0252	0.4654	0.5294
0.6137	0.0299	0.4936	0.5331
0.6530	0.0351	0.3200	0.5371
0.6898	0.0406	0.5447	0.5415
0.7241	0.0468	0.5675	0.5464
0.7560	0.0536	0.5891	0.5517
0.7860	0.0611	0.6091	0.5578
0.8139	0.0695	0.6279	0.5645
0.8402	0.0788	0.6461	0.5721
0.8655	0.0894		

Figure 3 - Diagram of Developed Top Surface Showing Layout for Construction of a Hollow Metal Float

in Figure 4. This float was used in the catenary-sweep application and represents the size and type used in the experiments described in this report.

The double tail fins are provided for directional stability, while the equiangular bridle, shown in Figure 2, is provided to maintain pitching stability. The function of the bridle is to permit stable towing when submerged as well as on the surface. The action of the bridle is illustrated by the following excerpt from Reference (2):

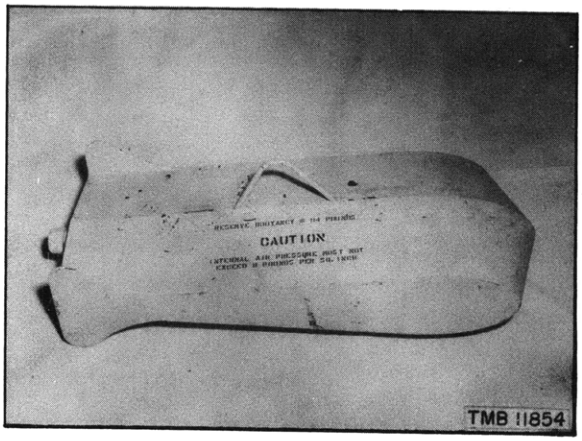

Figure 4 - TMB Planing Float

This float is of hollow sheet-metal construction, prestressed by internal air pressure. The pipe cap at the stern protects a check valve through which the internal pressure is applied. The lifting bail is shown on the top of the float.

> "When the float is towed by the bridle on the surface, both legs function when the float is carrying very large loads on the (tow)line. When the float is planing or carrying small loads, the forward leg is slack; the after leg carries the entire load. When the float is towed submerged, the line of action of the towline at the apex of the bridle passes between the two legs, so that the effective point of attachment of the cable is moved forward of the rear leg. The float stalls if towed with a single line to the after bridle point of attachment ... The equiangular bridle was selected as giving good performance both on the surface and completely submerged."

To meet the requirements of both weight and buoyancy it was necessary to use all-steel construction for the catenary-sweep application. Thus, unlike previous floats of this type which were made solid of white pine, the

floats for catenary sweeps were constructed of 0.072-inch sheet steel with a 3/8-inch steel plate as trimming ballast at the stern. These floats are 41 inches long and weigh 54.9 pounds in air, with a reserve buoyancy of 94 pounds per float.

The possibility of submergence of a float during service had to be considered, and the structural strength needed to meet this contingency had to be provided. The use of bulkheads inside the float was impracticable because of the resulting increase in weight and the reduction of reserve buoyancy. For these reasons, it was decided to use a hollow float reinforced by thin rods and prestressed by internal air pressure. The details of the construction and the results of tests to determine the maximum allowable depth of submergence are discussed in Appendix 3.

SUMMARY OF PREVIOUS DATA AVAILABLE FOR THE TMB PLANING FLOAT AND PURPOSE OF PRESENT TESTS

The results of previous tests to determine the load-carrying characteristics of the TMB planing float are reported in Reference (2). These tests were designed to provide data for maximum loading conditions. As a result, the float was tested under loads that are much greater than those encountered in the usual applications of planing surfaces. Under light loads at any speed or with moderate loads at high speeds, the float develops sufficient dynamic lift due to the fluid reaction on the bottom surfaces to allow full planing action with no contribution from the reserve buoyancy.

Under large loads, the float submerges slightly so that a sheet of water flows over the top. This condition induces dynamic lift as on a symmetrical airfoil, in addition to the reserve buoyancy. Under these conditions the lift-drag ratio, including the lift due to buoyancy, was found to be 3.0; the average trim angle was about 15 degrees. The tests showed that the float was able to carry a load of $0.625qb^2$ in addition to its own weight W. Here $q = \frac{1}{2}\rho v^2$, ρ is the mass density of the fluid in slugs per cubic foot, v is the towing speed in feet per second, and b is the beam of the float in feet. Thus the safe maximum lifting capacity L of the TMB float when operating as a surface buoy is given by

$$L = 0.625qb^2 + W \qquad [1]$$

The float was also tested as a fully submerged hydrofoil. In this condition the trim angle, or angle of attack, was found to be 28.5 degrees, and the drag D was given by

$$D = 0.83qb^2 \qquad [2]$$

The total vertical lift, dynamic and hydrostatic, was found to be

$$L = 1.44qb^2 + B \qquad [3]$$

where B is the total buoyancy or hydrostatic lift. The large angle of attack attained by the float in the submerged condition without stalling is attributed to its low aspect ratio (4).

Although these data were sufficient for designing an optimum surface float under given loading conditions, it was not possible to predict accurately the performance of the float in the planing regime. Therefore the tests of the float for the catenary-type minesweeping arrangement were extended to fill in the missing data. Since the tests were planned originally to provide a rapid check on the application as catenary-sweep floats, it was not considered expedient to develop dynamometers for the single design. However, the data proved to be sufficiently accurate to justify the use of the technique described in the following paragraphs in completing a definite program. A similar technique, which proved entirely reliable and on which the present method is based, is described in a report on the NRL Mark 3 buoy, Reference (5).

TEST METHODS AND TECHNIQUES

In tests of the NRL Mark 3 buoy (5), the maximum loading capacity under loads which increased with an increase in speed had to be determined. For this purpose, a carefully calibrated depressor was suspended below the buoy. The shape of the buoy was such as to give sharply defined combinations of loads and speeds at which the buoy became overloaded. For the TMB planing float, on the other hand, it was desired to determine the resistance and behavior under approximately constant loads over a considerable range of speeds. The tests were further complicated by the difficulty of determining the speeds at which true planing was obtained.

Based on the method used in testing the NRL Mark 3 buoy, a series of faired weights (or depressors) was designed for the application of the desired loads. The weights were designed to provide a family of loading curves with sufficient separation to cover the range of loads and speeds desired without exceeding the initial reserve buoyancy of the model tested. The four weights, shown in Figure 5, could be towed from either of two towpoints. For reasons of stability and to provide a slight negative angle of attack, the center of gravity of each weight was placed forward of the forward towpoint. The purpose of the negative angle of attack was to provide additional downward lift in order to counterbalance the upward lift forces on the weight towline.

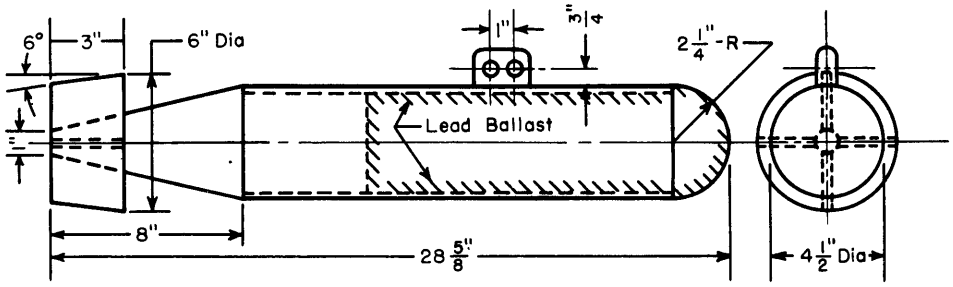

Figure 5a - 100-Pound (Nominal) Faired Weight

This weight weighs 102.0 pounds in air and 87.8 pounds in water.

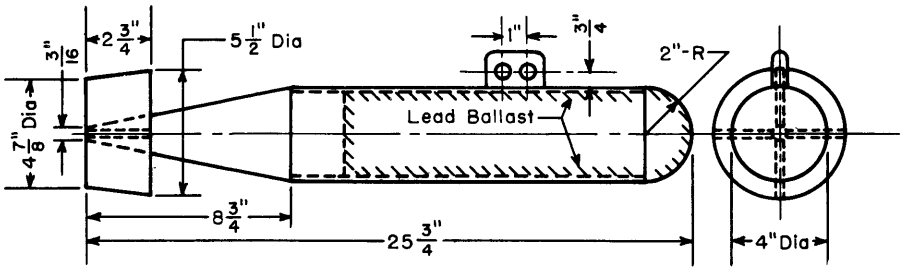

Figure 5b - 75-Pound (Nominal) Faired Weight

This weight weighs 70.4 pounds in air and 61.6 pounds in water.

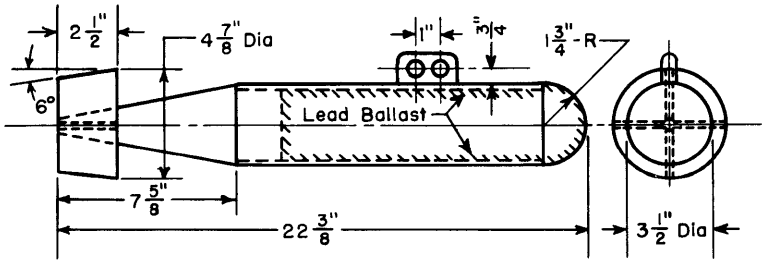

Figure 5c - 50-Pound (Nominal) Faired Weight

This weight weighs 47.4 pounds in air and 41.4 pounds in water.

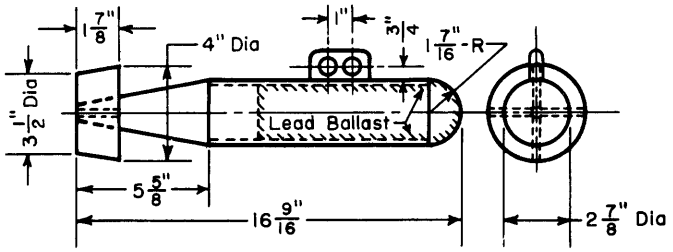

Figure 5d - 25-Pound (Nominal) Faired Weight

This weight weighs 24.7 pounds in air and 21.5 pounds in water.

Figure 5 - Dimensions and Weights of Faired Weights

Each faired weight was first carefully calibrated by towing it at the end of a line which was adjusted during the test to maintain a constant length from the towpoint on the weight to the water surface throughout the speed range. Towlines of the same length and size were subsequently used in the float tests. Each weight was towed from its two towpoints to obtain a series of loading curves for the float tests. The method of calibrating the weights is illustrated in Figure 6. The towline was led through a pulley at

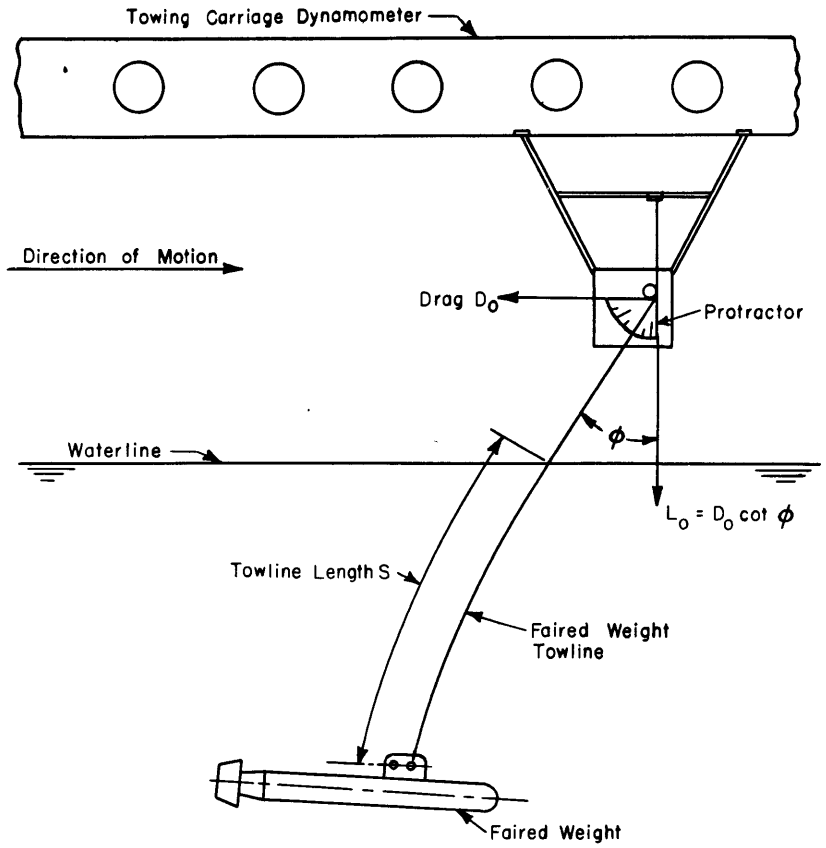

Figure 6 - Test Method for Calibration of Faired Weights

the center of a protractor and secured to the drag dynamometer on the towing carriage. The drag of the weight with its towline and the angle of the towline at the surface were measured over a range of speeds for each towpoint. From these measurements, the lift L_0 of the weight was computed from the equation

$$L_0 = D_0 \cot \phi \qquad [4]$$

where D_0 is the drag of the weight and its towline and ϕ is the angle of the towline with the vertical at the water surface. The results of the calibrations are shown in Figures 7 and 8. The drag curves obtained for the faired

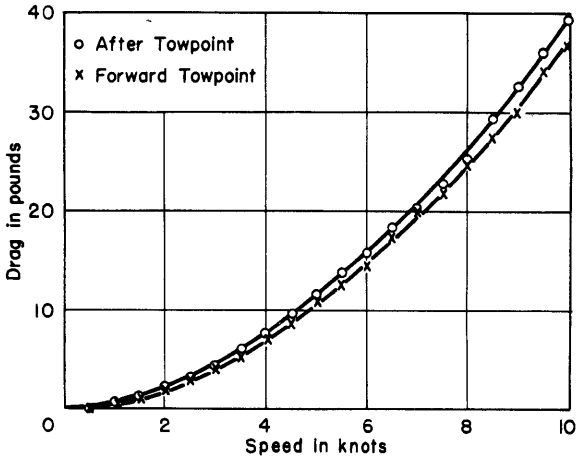

Figure 7a - 100-Pound Weight

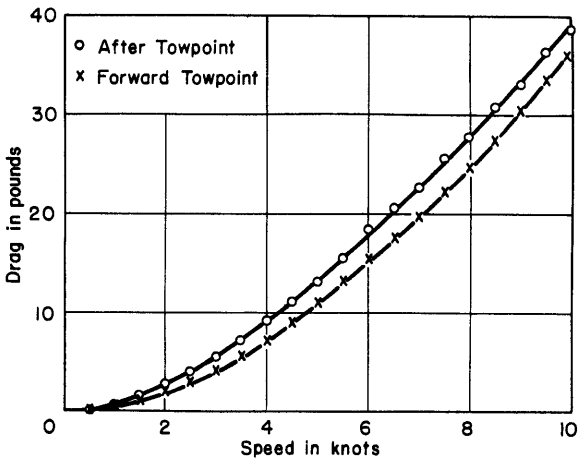

Figure 7b - 75-Pound Weight

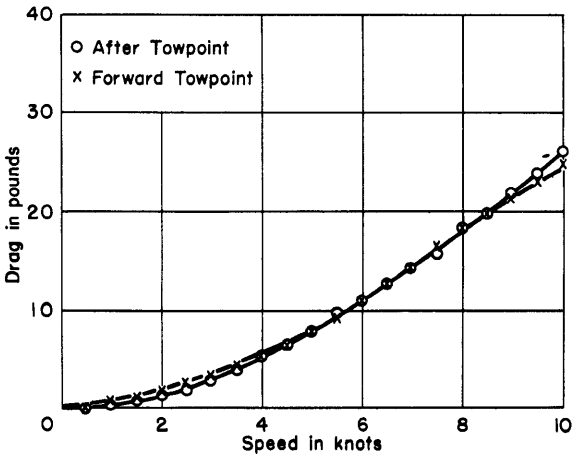

Figure 7c - 50-Pound Weight

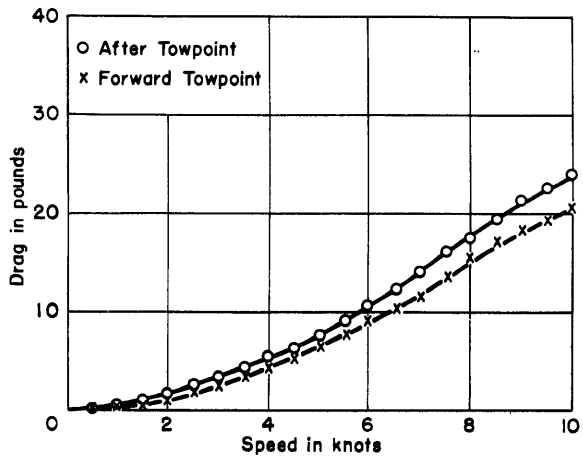

Figure 7d - 25-Pound Weight

Figure 7 - Drag Characteristics of Faired Weights

weights are shown in Figure 7. The 100-pound and 75-pound weights were each towed with 6.0 feet of flexible aircraft cable, 1/8 inch in diameter; the 50-pound and 25-pound weights were each towed with 6.0 feet of cable, 1/16 inch in diameter. The corresponding loading curves are shown in Figure 8.

The characteristics of the TMB planing float were obtained in the manner illustrated in Figure 9. The line used for towing the system was secured to the towing carriage dynamometer at the center of a protractor. The drag of the system and the inclination of the towline at the protractor were measured over a range of speeds and with the various faired-weight loading conditions. Since the shape and orientation of the line towing the weight remains the same for a given length and size of line at each speed, the weight calibrations could be used directly. The drag D of the float, then,

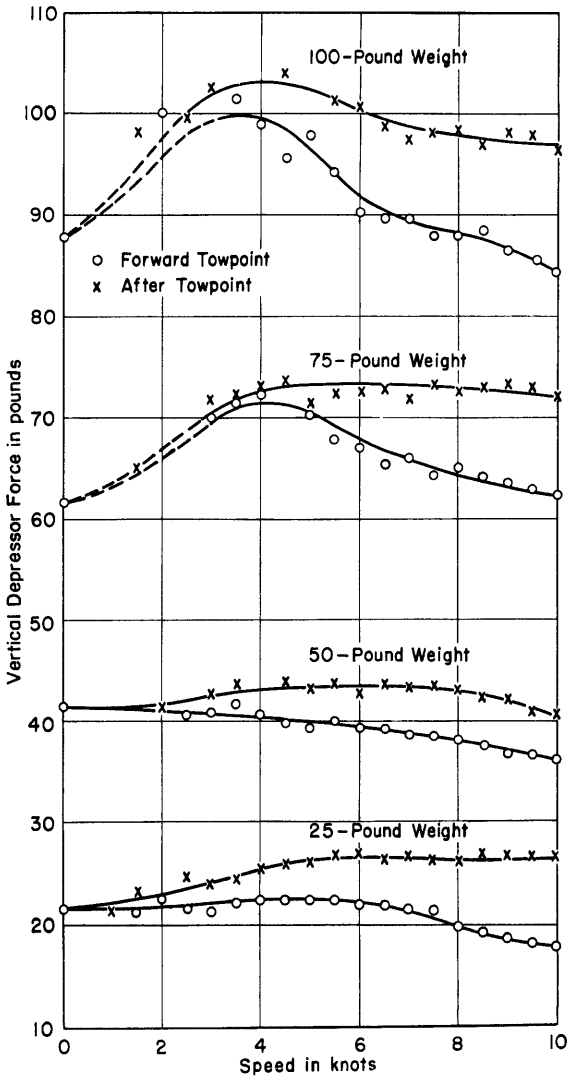

Figure 8 - Loading Curves Obtained from Faired-Weight Calibrations

is the difference between the measured drag F of the system and the drag D_0 of the weight and its towline as read from the calibration curve, or

$$D = F - D_0 \qquad [5]$$

Since a long line was used for towing the system, the angles made by this line at the protractor were of the order of 5 to 8 degrees from the horizontal. As a result, the fluid force on the cable was primarily tangential drag. Since the cable diameter was only 1/16 inch, this force and the curvature of the cable could be neglected in the analyzis of the data.

The load on the float consists of its own weight and the algebraic sum of the vertical components of the tensions in the faired weight and forward towlines, i.e.,

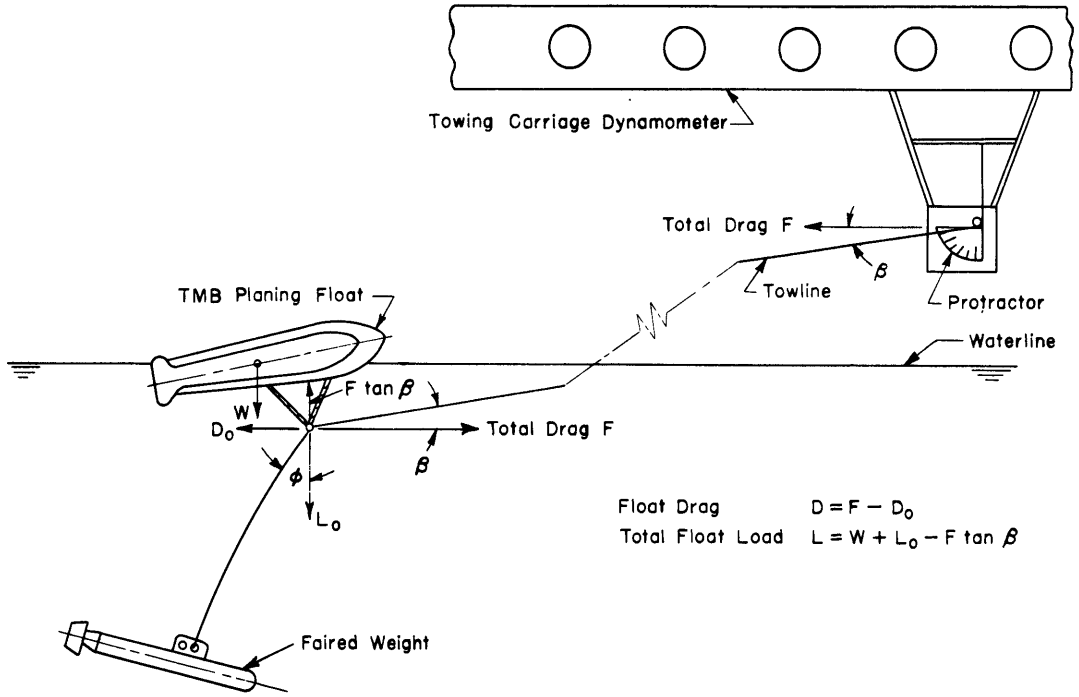

Figure 9 - Test Method for Determination of Characteristics of TMB Planing Float

$$L = W + L_0 - F \tan\beta \qquad [6]$$

where L is the total load on the float,

W is the total weight of the float, and

β is the angle of the float towline with the horizontal.

Here again the fluid forces on the line for towing the system were neglected.

RESULTS OF TESTS OF TMB PLANING FLOAT UNDER VARIOUS LOADING CONDITIONS

The series of tests discussed herein were conducted with a planing float 41 inches in length designed for the catenary sweep. The complete dimensions of this float are given in Figure 41, Appendix 3. The float was tested alone at a constant load of 54.9 pounds imposed by its own weight and under eight conditions of variable loading, imposed in part by the faired weights, Figure 8.

The results of the tests are plotted in Figure 10 as curves of drag in pounds against speed in knots for the various conditions of loading. Photographs of the float taken during these tests are shown in Figures 11 through 19.

From Figures 11, 12, and 13, it can be seen that the float did not become submerged for the conditions of no load and of the load imposed by the

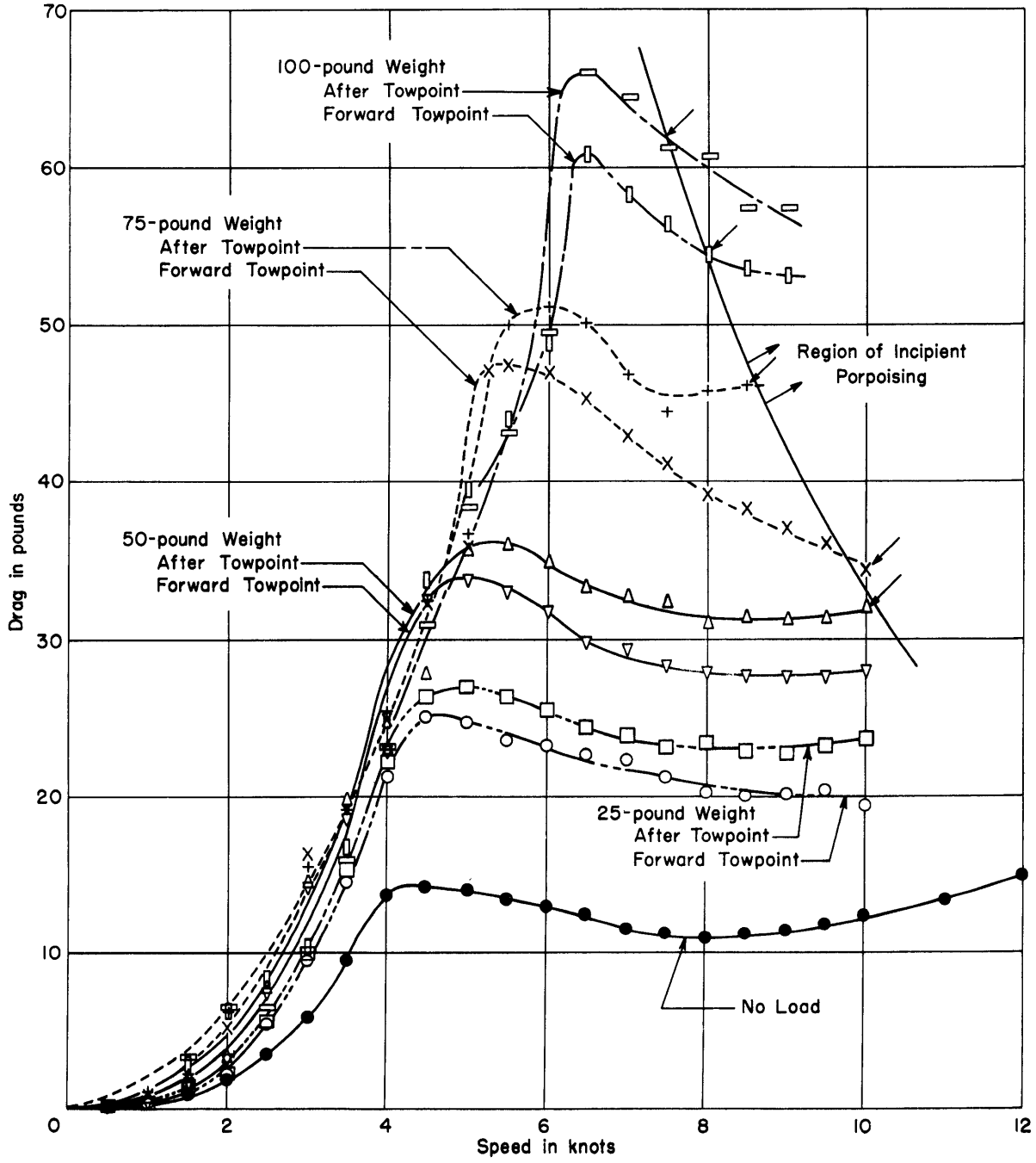

Figure 10 - Drag Curves for TMB 41-Inch Planing Float

25-pound faired weight. For greater loads, Figures 14 through 19, the float became submerged at relatively low speeds and later emerged at speeds near the humps in the curves of Figure 10. In general, under conditions of loading less than those imposed by the 100-pound weight, the float emerged just below the hump. However, some ambiguity exists as to the actual speed at

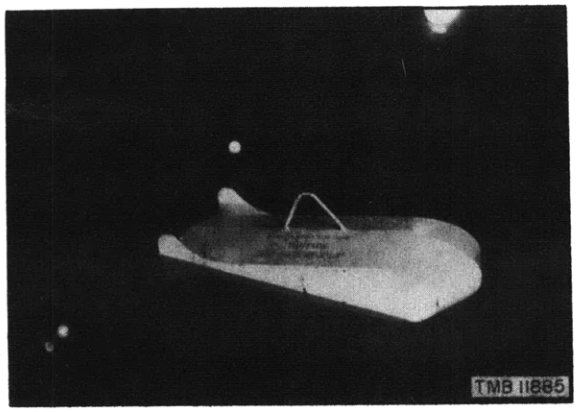

Towing Speed, 0.5 Knot

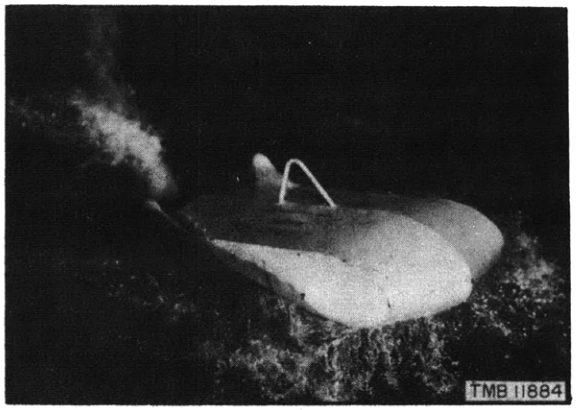

Towing Speed, 4.5 Knots

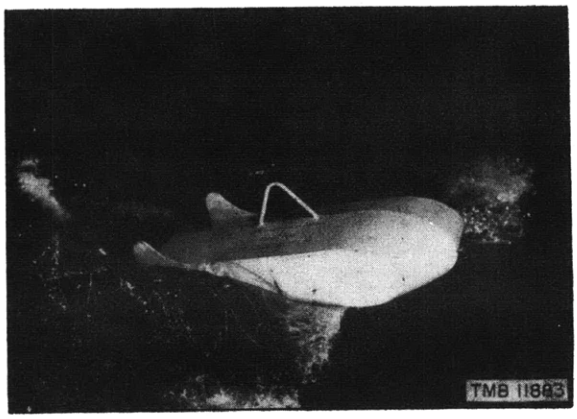

Towing Speed, 6.0 Knots

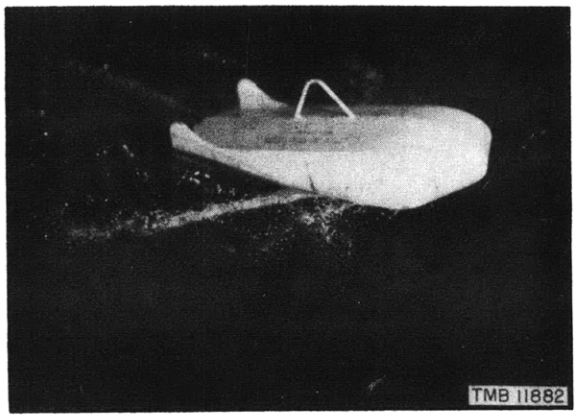

Towing Speed, 10.0 Knots

Figure 11 - Photographs of TMB 41-Inch Planing Float Being Towed

These tests were made under no imposed load.

which the float may be considered as having emerged. This will be shown in a subsequent discussion of transition from subsurface to surface operation.

The action of the float at the low speeds and its subsequent rising to the surface can be easily understood from an examination of the forces acting on the float form. At the low speeds, the flow around the float is primarily of the displacement type, and the load-carrying capacity of the float is due only to its buoyancy. However, because of the curvature of the bottom surfaces, local velocities higher than the speed of tow are induced, accompanied by a resultant pressure drop along the bottom. The pressure distribution is then such as to produce a downward component of force on the float and, consequently, an increase in draft (5). For no load and for the loading conditions obtained with the 25-pound weight, this force was not sufficient to submerge the float completely before it developed dynamic lift

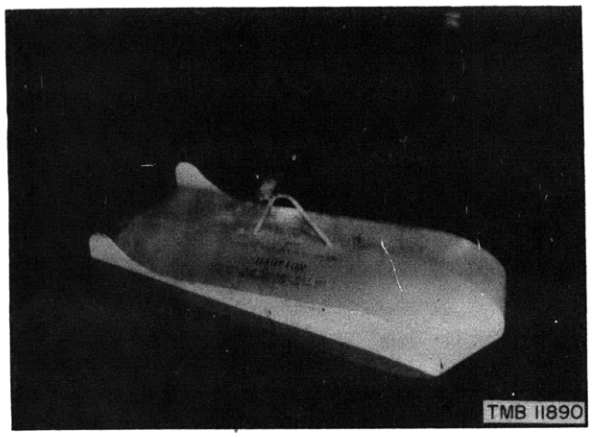

Towing Speed, 0.5 Knot

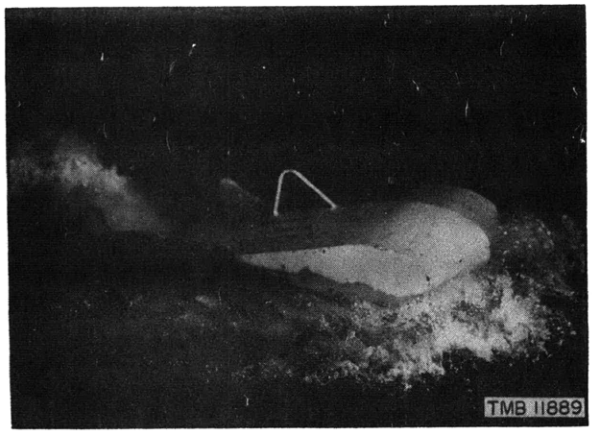

Towing Speed, 4.5 Knots

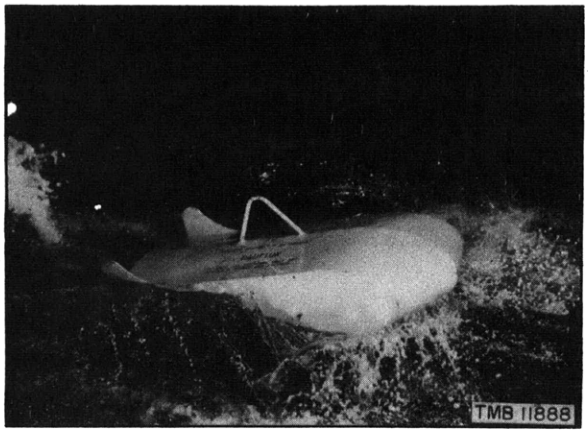

Towing Speed, 6.0 Knots

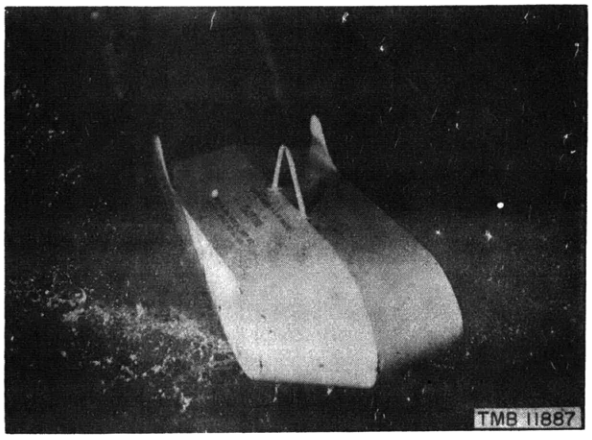

Towing Speed, 9.0 Knots

Figure 12 - Photographs of TMB 41-Inch Planing Float Being Towed

These tests were made under loads imposed by the 25-pound weight towed from the forward towpoint.

due to planing action. Under higher loads, however, the pressure reduction on the bottom surfaces was sufficient to submerge the float completely.

As the float becomes submerged, it begins to develop dynamic lift as a hydrofoil of low aspect ratio. Based on systematic tests of various hydrofoils at several depths of submergence (6), the dynamic lift on the float may be expected to show an increase up to a depth of about 5 chord lengths, at which depth the lift is fully developed to its maximum value. The maximum lift is then given by Equation [3], page 7, as determined from tests previously reported. In the tests considered here, the load on the float remained within definite limits as the speed was increased. As a result, the float assumed an equilibrium position below the water surface at each speed, until, with increasing speed, it developed sufficient lift as a hydrofoil to return to the surface.

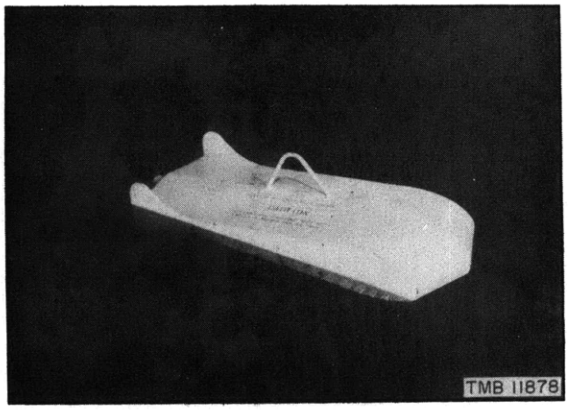

Towing Speed, 0.5 Knot

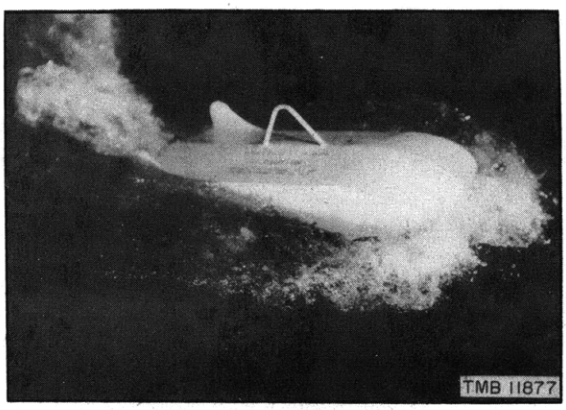

Towing Speed, 4.5 Knots

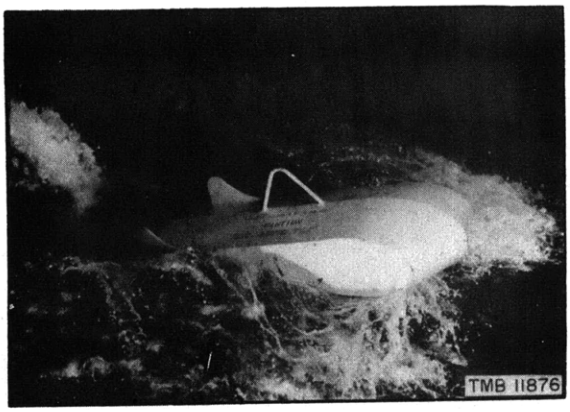

Towing Speed, 6.0 Knots

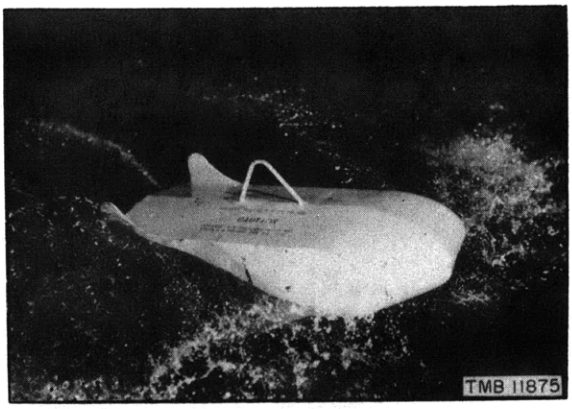

Towing Speed, 8.0 Knots

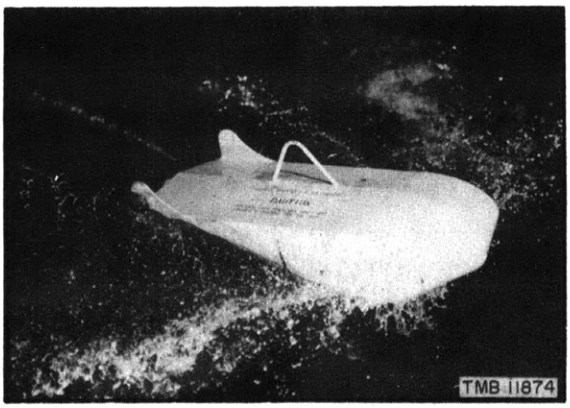

Towing Speed, 10.0 Knots

Figure 13 - Photographs of TMB 41-Inch Planing Float Being Towed

These tests were made under loads imposed by the 25-pound weight towed from the after towpoint.

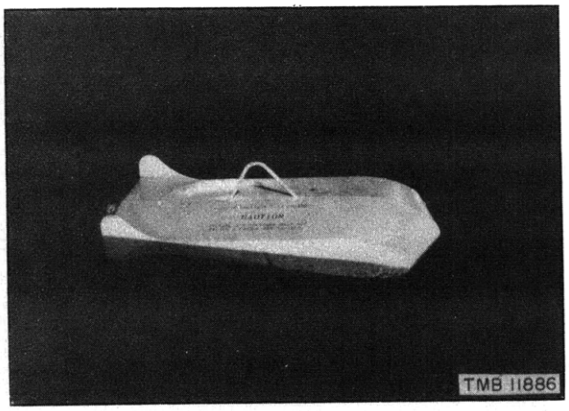

Towing Speed, 0.5 Knot

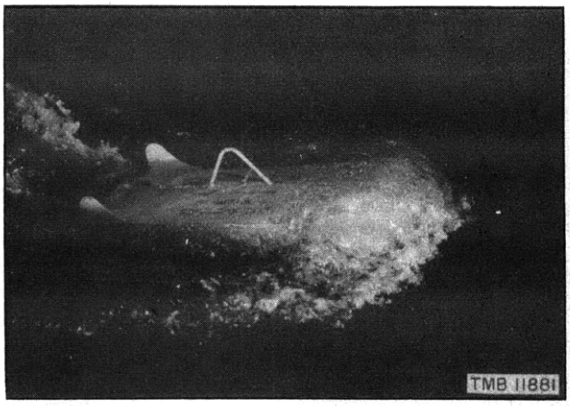

Towing Speed, 4.0 Knots

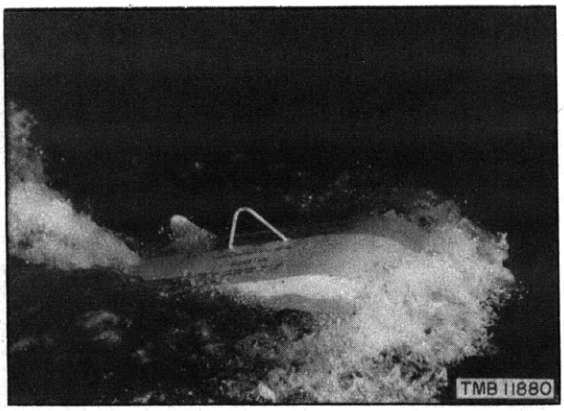

Towing Speed, 4.5 Knots

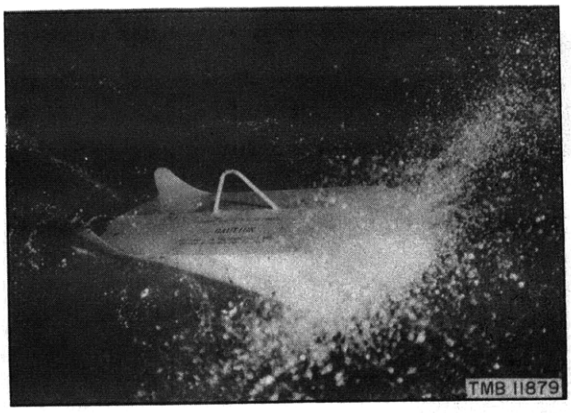

Towing Speed, 9.0 Knots

Figure 14 - Photographs of TMB 41-Inch Planing Float Being Towed

These tests were made under loads imposed by the 50-pound weight towed from the forward towpoint.

Throughout the submerged region, the drag of the float varies roughly as the square of the speed. At low speeds, for the loads under which the float does not become submerged, the drag is due primarily to skin friction and, in small part, to wave-making resistance, and varies as the speed to a power less than 2. At speeds that are sufficiently high, the float develops dynamic lift on the surface in addition to its buoyancy until it reaches the "hump" speed characteristic of planing surfaces, beyond which the load-carrying capacity of the float is attributable almost wholly to planing action. Just where the float reaches true planing action beyond the hump is difficult to determine. However, for purposes of the analysis made in subsequent sections, the planing region was taken to be the region beyond the peaks of the humps in the drag curves of Figure 10.

In general, the TMB planing float was stable throughout the various tests made. However, for the loading conditions imposed by the 75-pound and

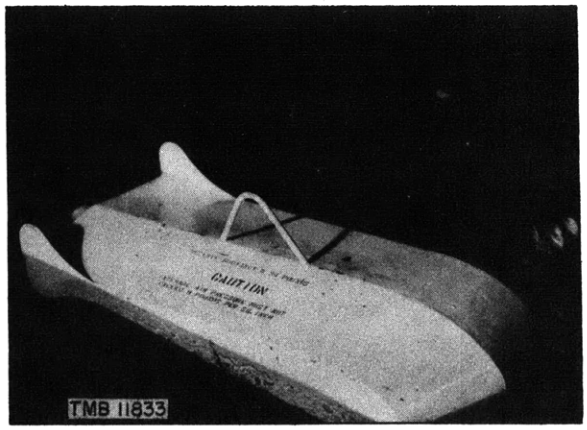

Towing Speed, 0.5 Knot

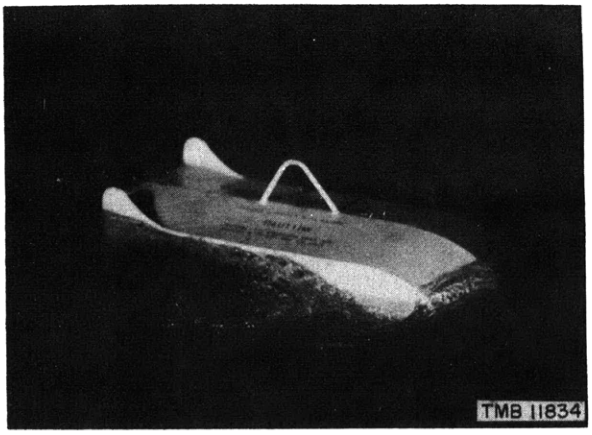

Towing Speed, 2.0 Knots

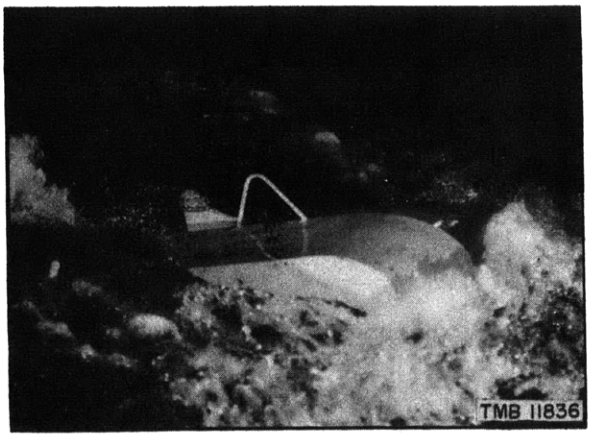

Towing Speed, 4.0 Knots

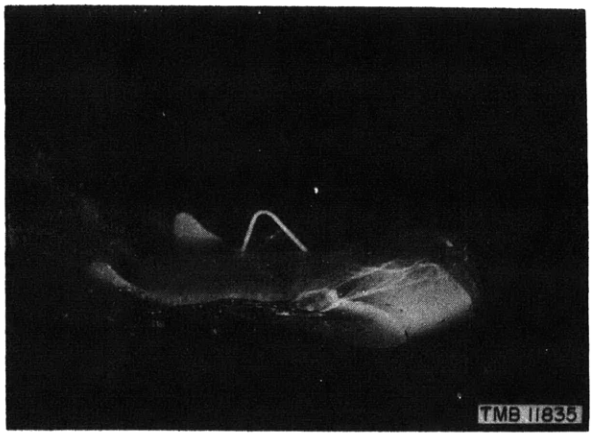

Towing Speed, 5.5 Knots

Figure 15 - Photographs of TMB 41-Inch Planing Float Being Towed

These tests were made under loads imposed by the 50-pound weight towed from the after towpoint.

100-pound faired weights at speeds as low as 7.5 knots, and for the loading conditions imposed by the 50-pound weight at speeds near 10 knots, the float showed a tendency to begin porpoising. As deduced from observations made during the actual tests, the speeds at which signs of porpoising appeared are indicated by the small arrows on the curves of Figure 10. The resulting smooth curve, shown on Figure 10 as the boundary of the region of incipient porpoising, is, however, somewhat misleading. Sometimes, especially for the highest loading condition, small oscillations in yaw were observed at speeds below this boundary. For the 75-pound weight, these oscillations appeared to become completely damped out before reaching the porpoising boundary. For the 100-pound weight, on the other hand, the oscillations became converted into a pitching motion and subsequent porpoising. If the end points at which the oscillations in yaw began and at which they were damped out were plotted

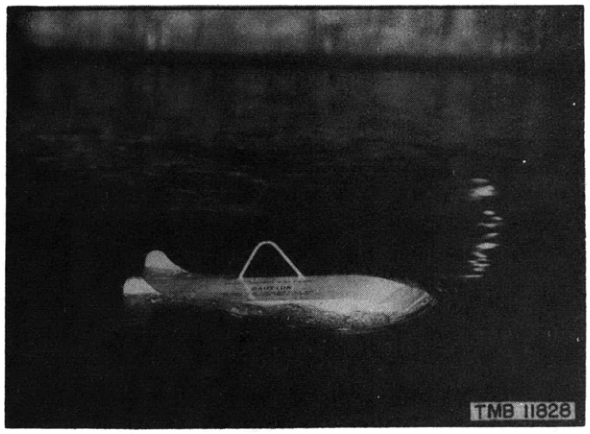

Towing Speed, 0.5 Knot

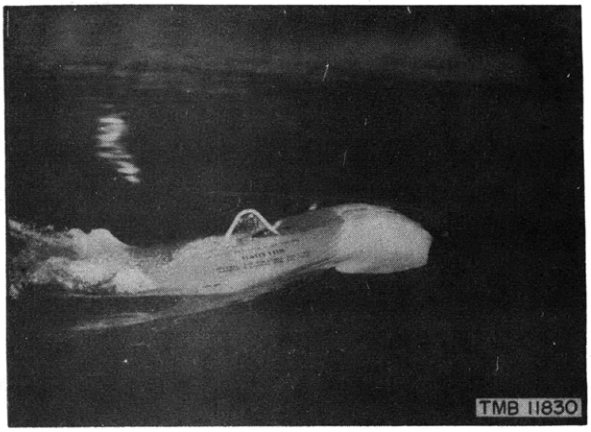

Towing Speed, 3.5 Knots

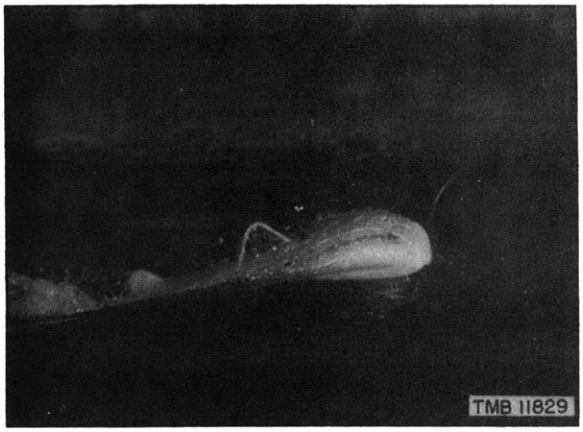

Towing Speed, 5.0 Knots

Towing Speed, 6.0 Knots

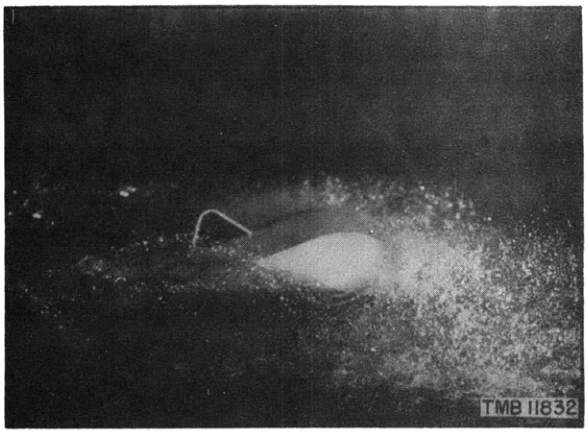

Towing Speed, 9.0 Knots

Figure 16 - Photographs of TMB 41-Inch Planing Float Being Towed

These tests were made under loads imposed by the 75-pound weight towed from the forward towpoint.

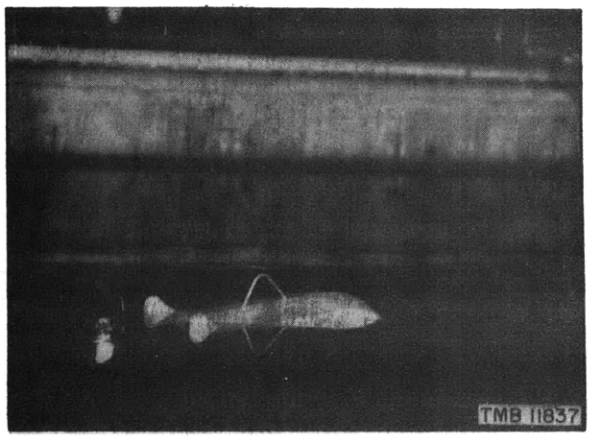

Towing Speed, 0.5 Knot

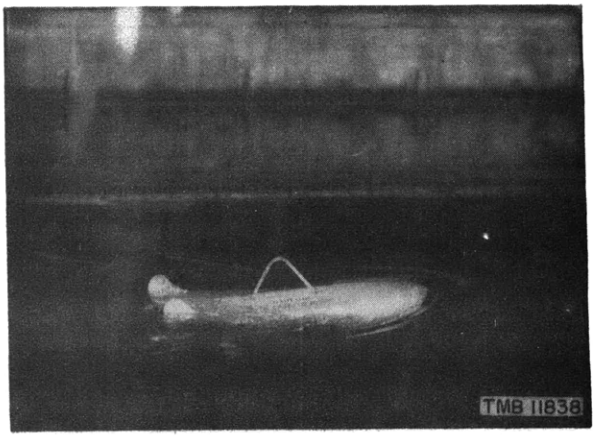

Towing Speed, 2.0 Knots

Towing Speed, 4.5 Knots

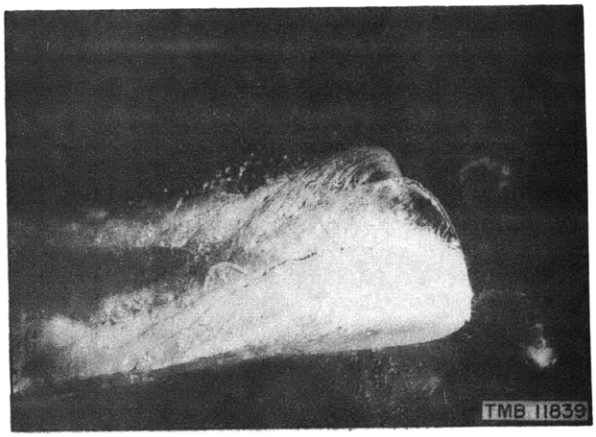

Towing Speed, 5.5 Knots

Figure 17 - Photographs of TMB 41-Inch Planing Float Being Towed

These tests were made under loads imposed by the 75-pound weight towed from the after towpoint.

on the curves of Figure 10, the result would be a closed contour starting beyond the humps and ending near the boundary of the porpoising region and lying above the curves for loading by the 50-pound faired weights. Since it was not possible to determine whether these oscillations were due to some instability in the faired weight, which was reflected in the motion of the float, or whether they were due to the float itself, they have been mentioned here without further attempt at analysis.

Furthermore, for all loads except the 75-pound weight towed from the after towpoint, fully developed porpoising failed to materialize. Under the load imposed by the 75-pound weight towed from the after towpoint, however, violent porpoising developed almost immediately in the region beyond the limiting curve of "incipient porpoising."

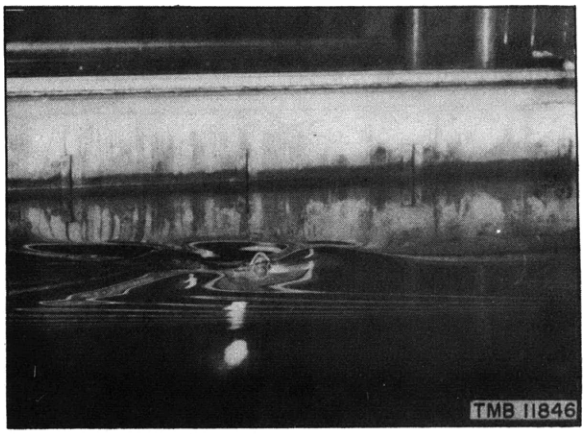

Towing Speed, 2.5 Knots

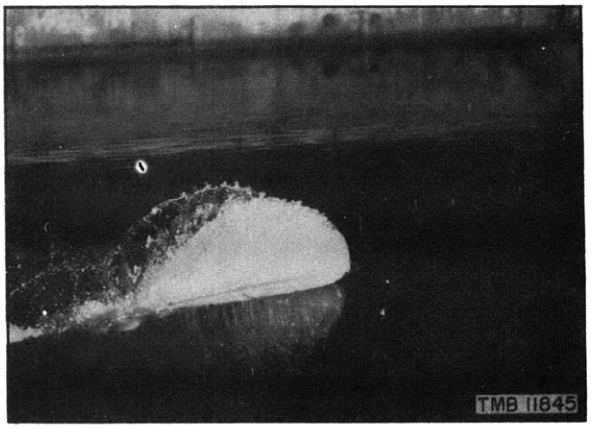

Towing Speed, 6.0 Knots

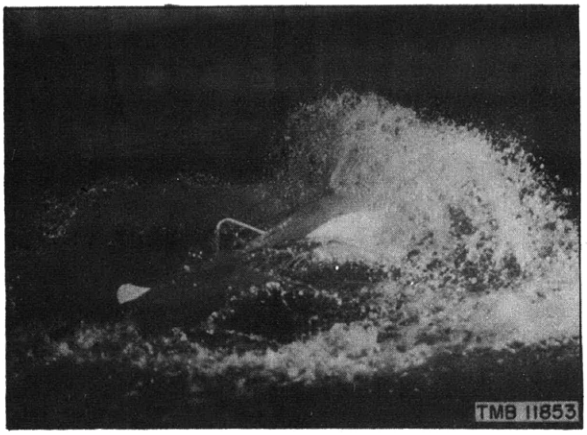

Towing Speed, 8.0 Knots

Figure 18 - Photographs of TMB 41-Inch Planing Float Being Towed

These tests were made under loads imposed by the 100-pound weight towed from the forward towpoint.

An indication of the magnitude of the oscillations that were observed near the region in which signs of porpoising appeared can be obtained from Figure 20. In this figure, the curves of variations in drag about the mean drag have been traced directly from the recording tapes on the carriage dynamometer. In the first three records at the top of the figure, no well-defined oscillations in pitch could be observed visually. For the remaining conditions, i.e., loads imposed by the 75-pound weight towed from the after towpoint, oscillations in pitch seemed to be very gentle when observed visually. However, the actual amplitude of the variation grows with speed, although the frequency appears to remain fairly constant. These curves probably do not represent accurately the actual modes of porpoising of a free float, in which the equivalent load is built into the float, because during the tests an effective spring action resulted from the curvature of the towing cable to the faired weight.

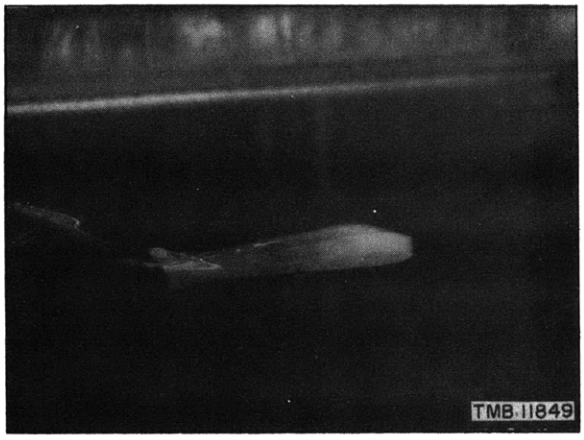

Towing Speed, 3.0 Knots

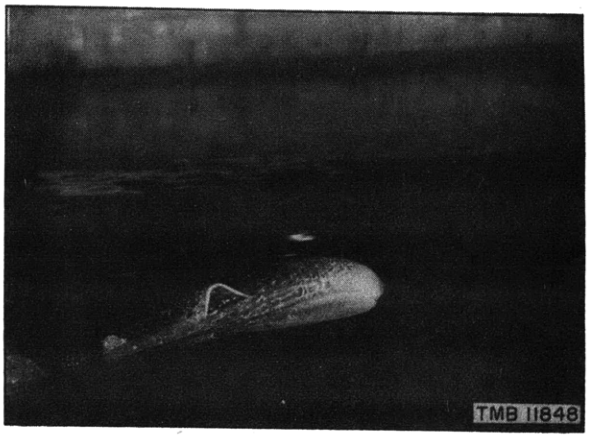

Towing Speed, 5.5 Knots

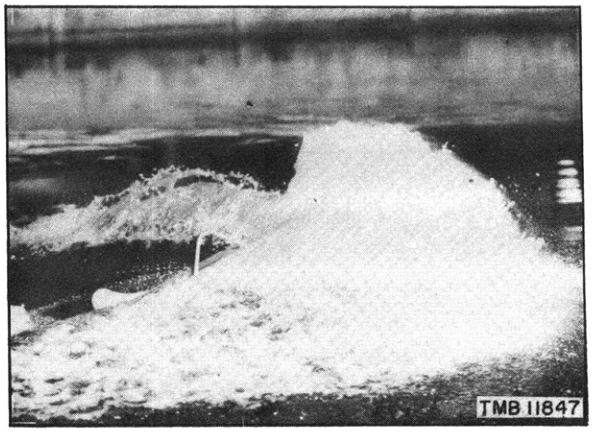

Towing Speed, 7.0 Knots

Figure 19 - Photographs of TMB 41-Inch Planing Float Being Towed

These tests were made under loads imposed by the 100-pound weight towed from the after towpoint.

Figure 20a - Drag under Load Imposed by 50-Pound Weight Towed from Forward Towpoint
Average drag, 27.90 pounds; Towing speed, 10.02 knots; Frequency, 1.14 cycles per second.

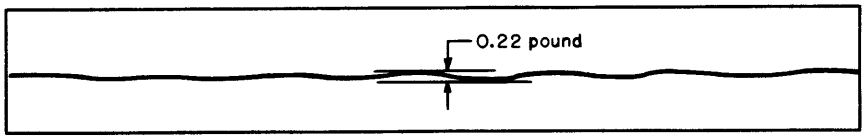

Figure 20b - Drag under Load Imposed by 50-Pound Weight Towed from After Towpoint
Average drag, 31.90 pounds; Towing speed, 9.99 knots; Frequency, 1.34 cycles per second.

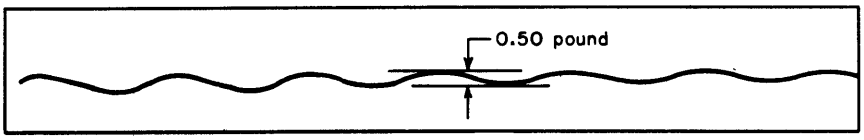

Figure 20c - Drag under Load Imposed by 75-Pound Weight Towed from Forward Towpoint
Average drag, 34.50 pounds; Towing speed, 9.98 knots; Frequency, 1.28 cycles per second.

Figure 20d - Drag under Load Imposed by 75-Pound Weight Towed from After Towpoint
Average drag, 44.35 pounds; Towing speed, 7.48 knots; Frequency, 0.95 cycles per second.

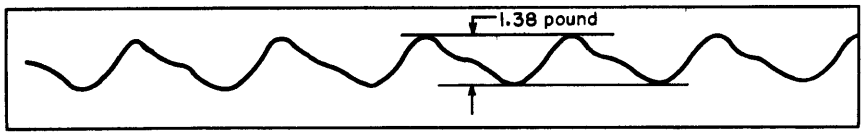

Figure 20e - Drag under Load Imposed by 75-Pound Weight Towed from After Towpoint
Average drag, 45.70 pounds; Towing speed, 8.00 knots; Frequency, 0.94 cycles per second.

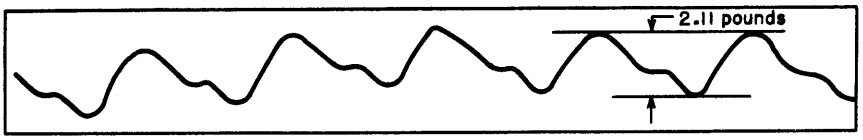

Figure 20f - Drag under Load Imposed by 75-Pound Weight Towed from After Towpoint
Average drag, 46.15 pounds; Towing speed, 8.50 knots; Frequency, 0.96 cycles per second.

Figure 20 - Examples of Cyclical Variation in Drag of the TMB Planing Float under Certain Load and Speed Conditions

THE HYSTERESIS REGION IN TRANSITION THROUGH THE AIR-WATER INTERFACE

Throughout the tests of the TMB planing float, it was noticed that the float exhibited unstable characteristics as it passed from subsurface to surface operation. Here the two conditions are defined in terms of the appearance of the flow about the float. If water continued to flow over the top of the float, the float was considered to be in the subsurface condition; when the flow changed so that spray was thrown forward and to the sides, the float was considered to be in the surface condition. However, unlike the NRL Mark 3 buoy (5), which has a sharp discontinuity at the intersection of the bottom surfaces and the deck and for which the speed of transition from subsurface to surface operation was sharply defined as based on the above criteria,* the speed at which the change occurs for the TMB float is not clearly defined. At the speed at which the TMB float passes through the air-water interface, an unstable condition occurs in which the water is alternately passing over the float and being thrown forward. During this condition, the float was observed at times to yaw sharply to one side. The cause of the yaw is attributable to small deviations from symmetry which produced slightly different flow conditions around the two sides of the float.

It was further observed, as can be seen in Figure 10, that under some conditions the beginning of the hump in the drag curve has a sharper curvature than under other conditions. Since the transition through the air-water interface begins at approximately this position, it was thought that there may be a hysteresis effect during the transition process. To test this hypothesis, careful experiments were made during which drag measurements and photographs of the flow were taken.

These experiments were made under loads imposed by the 100-pound weight towed from the forward towpoint. The measurements were made in two ways. To obtain measurements with the flow over the top of the float, the towing carriage was accelerated extremely slowly to the speed desired. If the carriage operator accelerated beyond the originally desired speed, he was instructed not to slow down to this speed, but to hold whatever speed he had attained. To obtain the type of flow in which water was thrown forward and to the sides, the carriage was run up to a speed well beyond the transition region and then decelerated very slowly to the speed desired. The results of these tests clearly showed the existence of the hysteresis region.

Photographs of the flow about the float obtained at two different speeds in this region are shown in Figure 21. The resistance of the float in

---

* The fact that this transition speed was so sharply defined for the NRL buoy made it possible to define its maximum load-carrying capacity on this basis.

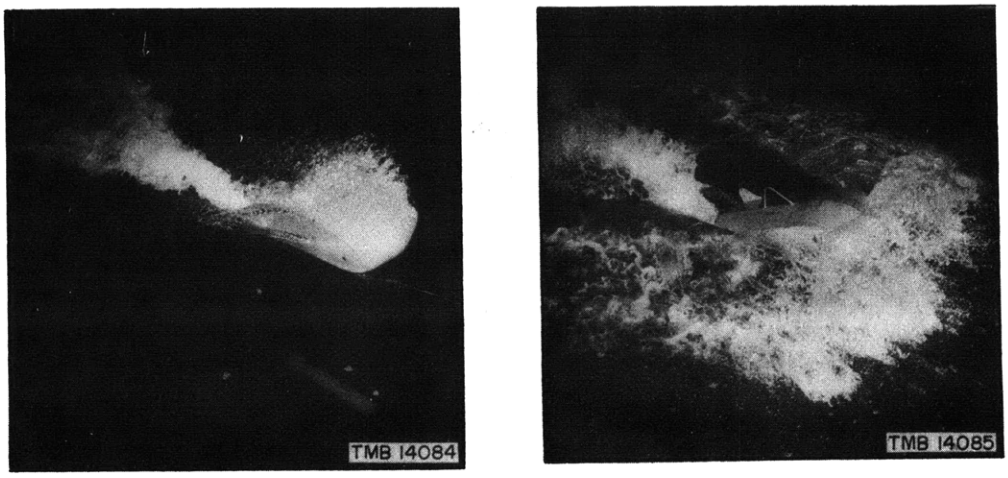

Figure 21a - Photographs of the Two Types of Flow at 5.94 Knots

In the photograph on the left, the float was accelerated to 5.94 knots; in the photograph on the right, the float was decelerated from a speed beyond the hysteresis region.

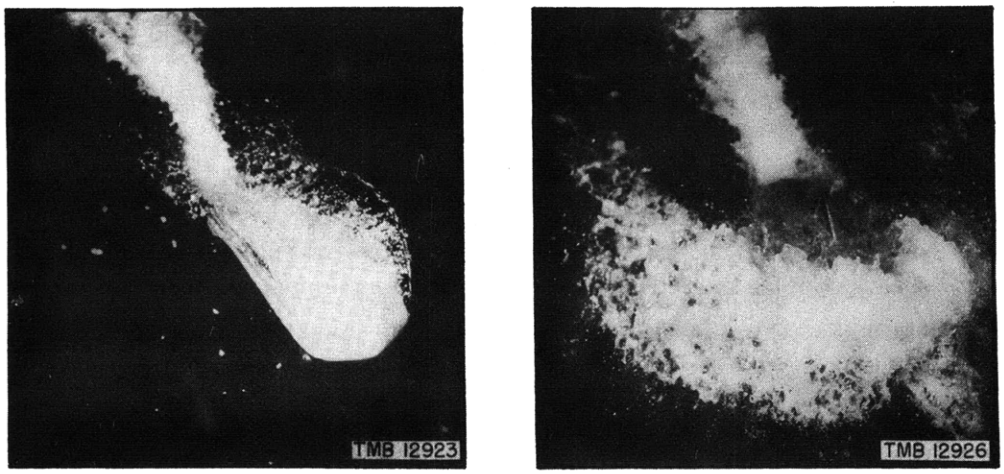

Figure 21b - Photographs of the Two Types of Flow at 6.20 Knots

In the photograph on the left, the float was accelerated to 6.20 knots; the photograph on the right shows the float just after it had suddenly yawed to its port side with a resultant breakdown of flow to the more stable type in which water is thrown forward and to the sides.

Figure 21 - Photographs of the Flow about the TMB Planing Float in the Hysteresis Region

These tests were made under loads imposed by the 100-pound weight towed from the forward towpoint.

this region, showing the hysteresis loop, is plotted in Figure 22. The photographs in Figure 21a, which were both taken at a speed of 5.94 knots, exhibit clearly the two possible types of flow in the hysteresis region. Near the entrance of the hysteresis loop, shown in Figure 22, conditions are least stable, and the flow tends to change from one type to the other. The flow in which water is thrown forward of the float, occurring on the upper branch of

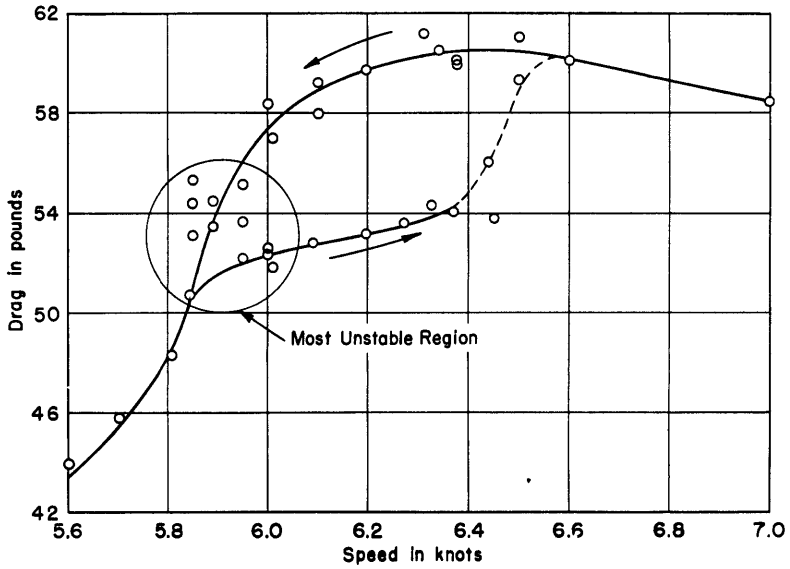

Figure 22 - Hysteresis Loop for TMB Planing Float under Load Imposed by 100-Pound Weight Towed from the Forward Towpoint

the loop in Figure 22, was shown to be the more stable of the two types; on the lower branch, any slight disturbance in the flow causes a complete breakdown over the top, and the flow goes over into the type in which the water is thrown forward. This is illustrated in Figure 21b, in which the flow while on the lower branch of the hysteresis loop broke down when the float yawed suddenly. The right-hand photograph of Figure 21b was taken immediately after this breakdown had occurred; the float had not quite returned to a straight course from its yawed position.

The conclusion can be drawn from these observations that the instability and probably also the hysteresis region will exist for any hydrofoil with a well-rounded leading edge, in transition through the air-water interface. It is possible that for a hydrofoil of much larger aspect ratio, for which the angles of attack must be kept small to avoid stalling, this instability may not manifest itself to the extent shown by the TMB float, which, in the submerged condition, may be considered as a thick hydrofoil of low aspect ratio. Furthermore, as was shown by the tests of the NRL Mark 3 buoy (5), the transition for a hydrofoil with a sharp leading edge is well-defined and occurs at a single speed. For this hydrofoil, the point of separation of flow is fixed at the leading edge and no hysteresis loop exists.

During the experiments in the hysteresis region, it was also found that striations appeared in the flow configuration while the water was still passing over the top of the float. A discussion of this phenomenon and an attempt to explain the formation of the striations follow.

A HYPOTHESIS FOR THE STRIATION PHENOMENON

It is interesting to observe that the flow over the float while it is still submerged and is being towed in a "cavity" formed in the water, exhibits the same type of striations near the points of separation, Figure 21a, as is shown by a sphere or projectile dropped through a free surface. A photograph of a sphere dropped into the transparent-wall tank at the Taylor Model Basin exhibits these striations clearly, as is shown in Figure 23. Similar striations also appeared during the tests of the balsa-wood displacement float; see Figure 32.

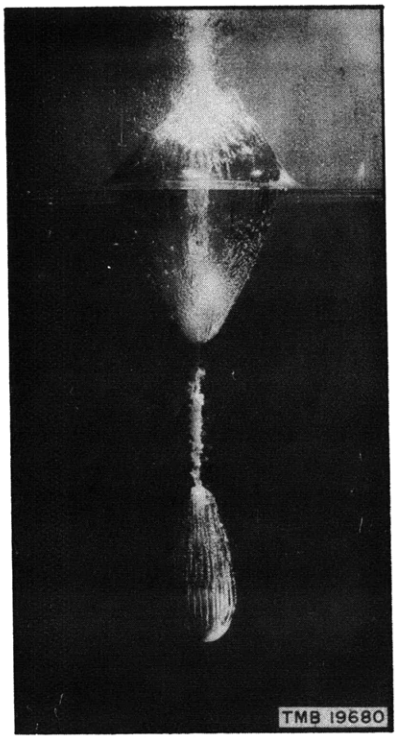

Figure 23 - Photograph of Aluminum Sphere Dropped into the Transparent-Wall Tank at the Taylor Model Basin

The entrance velocity was approximately 29 feet per second.

It has been suggested that the striations on a sphere dropped into water are the result of the formation of cavities about minute nuclei on or near the surface of the sphere. However, the very even spacing of the striations on the planing float, as well as on the sphere shown in Figure 23, suggests that a phenomenon other than that due simply to a random distribution of nuclei is more likely to be the cause of the configuration. Although the condition of the surface of the experimental specimen is undoubtedly an important variable in the flow configuration, as evidenced by many sphere drops

which do not show such clear definition as is evident in Figure 23, the resultant pattern appears to be a more complicated function of the surface roughness and of the flow conditions than would follow from the simplified assumption of cavitation formation about nuclei.

It is proposed to outline here a hypothesis which explains somewhat more satisfactorily the formation of the striations. It is known, see Reference (7), that conditions in the boundary layer near the point of separation of flow are such that a strong vortex is formed. If the vortex formation is a stable one, the flow should separate in a smooth sheet. For a flat plate, the conditions at separation can be considered as giving rise to a line vortex; while for the sphere or a body of revolution, such as the balsa-wood displacement float shown in Figure 32, the vortex can be considered as a ring. In order that striations may be formed at the point of separation, the vortex pattern must be altered so that a number of striations are formed depending on speed and on the strength of the vortex. That such conditions may arise can be seen by analogy with a free vortex ring generated in a fluid at rest.

An excellent series of experimental observations on the stability of vortex rings has been reported in Reference (8). In these experiments, vortex rings were generated in water at rest and were observed by means of dye filaments. Observations were made of the vortex ring shape both in cross section and plan on rings generated at various speeds of translation. The result of most interest to this discussion is the change in shape of the vortex ring shortly after its generation. It was shown that for a definite range of speeds of propagation, the circular ring is unstable. In cross section, the vortex core changes from a circular to an elliptical section and the entire ring assumes a polygonal shape with a number of evenly spaced deformations or waves. Photographs of two rings taken from Reference (8) are shown in Figure 24. The observations showed that the maximum diameter of the ring remains approximately constant but that the deformations form toward the inside of the ring. For very slow rings and for rings with a very high speed of propagation, these deformations were not observed. However, the number of discrete deformations in the ring increases with speed of propagation, the wave height decreasing as the number of deformations increase. In addition to these changes, the ring no longer remains plane but exhibits oscillations when viewed at right angles to the path of translation. The statement is further made in Reference (8) that the pressure at the peaks on the outside of the ring is lower than that at the inward peaks.

If, then, it can be assumed that a region of high vorticity exists near the point of separation, and, in the case of actual separation, a vortex does exist, the instability of the vortex can be expected to give rise to the type of deformation shown by the vortex ring with the resultant configuration

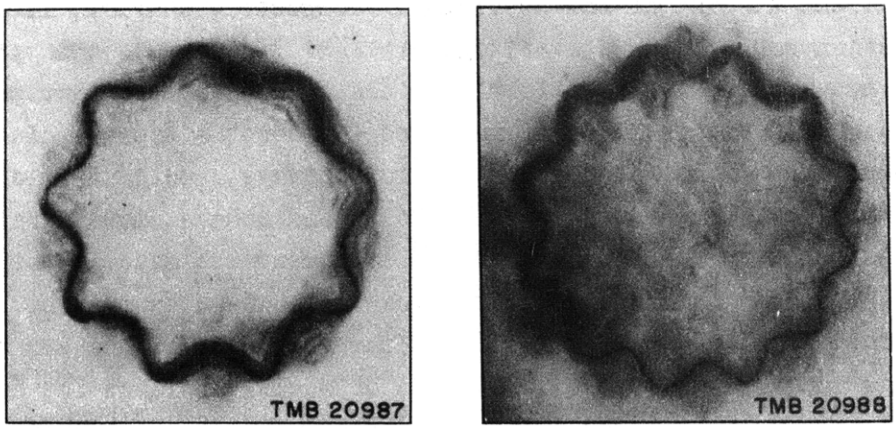

Figure 24 - Photographs of Stabilized Vortex Rings

These photographs were taken from Reference (8).

observed on the floats and sphere drops. On the basis of these remarks, it appears that these striations should be existent in the fluid whether cavitation has begun or not. That they have not been observed at pressures above the cavitation pressure may be due to the necessity of having a "free" surface to provide a reflecting surface for the light used in photographs or in visual observations. As a corollary to these conclusions, the presence of striations evidently indicates that flow separation has taken place upstream from the position at which the striations are observed.

Although separation usually occurs in the region of increasing pressure just beyond the minimum-pressure point, the pressure in the vortex, which can be lower than the minimum pressure on the body, may allow cavitation to be observed first in the vortex. Since the lower pressure occurs at the outside peaks in the deformed vortex, these points may be expected to cavitate first or, at least, to give larger cavitation pockets than the inner peaks, resulting in striations when observed under proper lighting conditions. Since a high degree of vorticity is convected downstream from the point of separation, it may be expected that a corrugated vortex sheet will be maintained until the vortex sheet is dissipated.

Returning to a consideration of the vortex ring, the deformation should undergo oscillations along radii from the center of the ring, and, as a matter of fact, this can be observed with ordinary smoke rings in undisturbed air. Unless the configuration is stabilized under cavitating conditions, it should be possible to observe an oscillation of the striations in directions perpendicular (radial and, therefore, also tangential) to the path of the specimen. However, it is possible that nonuniformity of the surface would obscure or upset such oscillations.

If the surface of the specimen is completely uniform, it appears that separation would occur at a fixed, *straight* line around the specimen and that the striations would be uniformly spaced. However, the photograph of the sphere drop in Figure 23 by no means represents the typical distribution on all sphere drops. Although the striations always appear, they are seldom as uniformly distributed as on the floats and sphere shown herein. It is in connection with this point that the statement was made in the foregoing that the surface roughness is undoubtedly a variable which must be considered in explaining the flow configuration. If the roughness of the surface is not uniform, the idea of a random distribution of nuclei explains the ragged line of separation. The result would be a vortex of nonuniform strength with resulting distortion of the striation pattern.

So far the discussion has been concerned only with examples in which the pressure in the "cavity" behind the specimen is atmospheric. However, the same results should be manifested when the cavity is closed and the pressure within it is lower. That the same results actually occur has been observed in photographs of torpedo models under cavitating conditions in the variable-pressure water tunnel.

ANALYSIS OF THE DATA IN THE PLANING REGIME

The principal purpose of the present investigation was to extend the available data for the TMB planing float into the planing regime. Owing to the techniques of experimentation used, any attempt to deduce criteria from the data below the hump speed would prove fruitless because of the number of variables that must be taken into account when the float is completely submerged at undetermined positions below the surface. Furthermore, the results reported previously for maximum loading (2) are sufficient for design purposes below the hump speed.

With the methods used, it is not possible to determine precisely the speed at which true planing begins. Inasmuch as the effects of displacement and of dynamic lift on the float occur together in a region of transition from typical displacement flow to true planing, the definition of the boundary between the displacement regime and the planing regime is arbitrary. For purposes of the reduction of the TMB float data, this dividing line is defined as the speed determined by the position of the horizontal tangent to the drag curve at the hump. This definition is not entirely satisfactory because of the ambiguity existing in the hysteresis region for the heavy load conditions, but the data can be reduced to a unique relationship on this basis.

Using the horizontal-tangent method on all the drag curves of Figure 10, the dividing line between the displacement and planing regime is shown by

the points on Figure 25. Assuming the load to vary as the square of the speed for these points, a good fit is obtained by the parabola

$$L = 3.57\ V_P^{\,2} \qquad [7]$$

where L is the total load (applied load plus the weight of the float) in pounds and V_P is the speed determined by the horizontal tangent at the hump in knots. Defining a nondimensional load-carrying or lift coefficient C_L by

$$C_L = \frac{L}{\frac{2.85}{2}\rho V^2 b^2} \qquad [8]$$

where ρ is the mass density of the fluid in slugs per cubic foot,

V is the speed in knots,

b is the beam of the float in feet, and

2.85 is the factor for converting the square of the velocity in knots to the square of the velocity in feet per second,

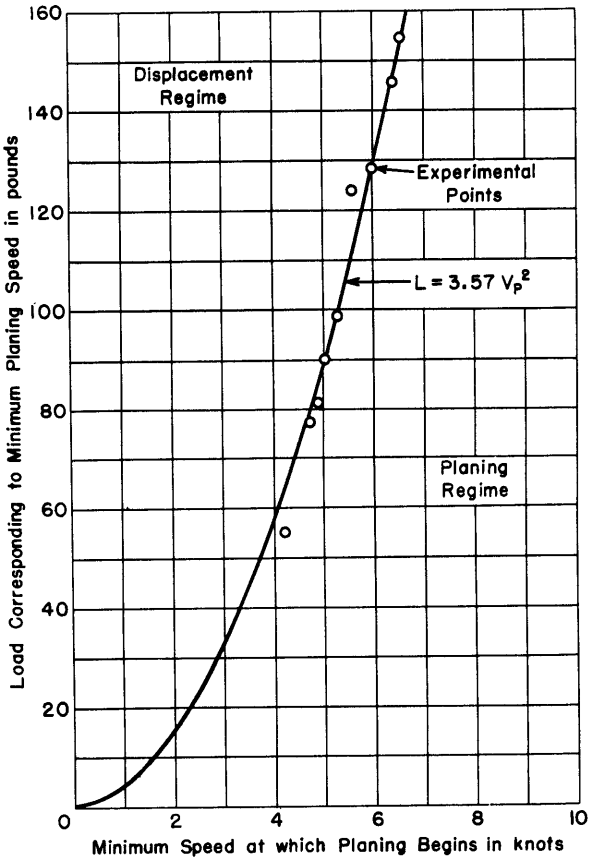

Figure 25 - Definition of the Displacement and Planing Regimes for the TMB Planing Float

the float will operate in the planing regime at all values of $C_L \leqq 0.69$.

At speeds above the hump and for the scale of floats likely to be designed on the basis of these data, the observed drag can be expressed by a functional relationship of the type

$$C_D = C_D\left(C_L, \frac{V}{\sqrt{b}}\right) \qquad [9]$$

Here the nondimensional drag coefficient C_D is defined as

$$C_D = \frac{D}{\frac{2.85}{2}\rho V^2 b^2} \qquad [10]$$

where D is the drag of the float in pounds and the other variables are as defined in the foregoing.

Equation [9] is represented by the graphs of Figure 26, in which values of C_D are plotted on a basis of C_L at constant values of the parameter

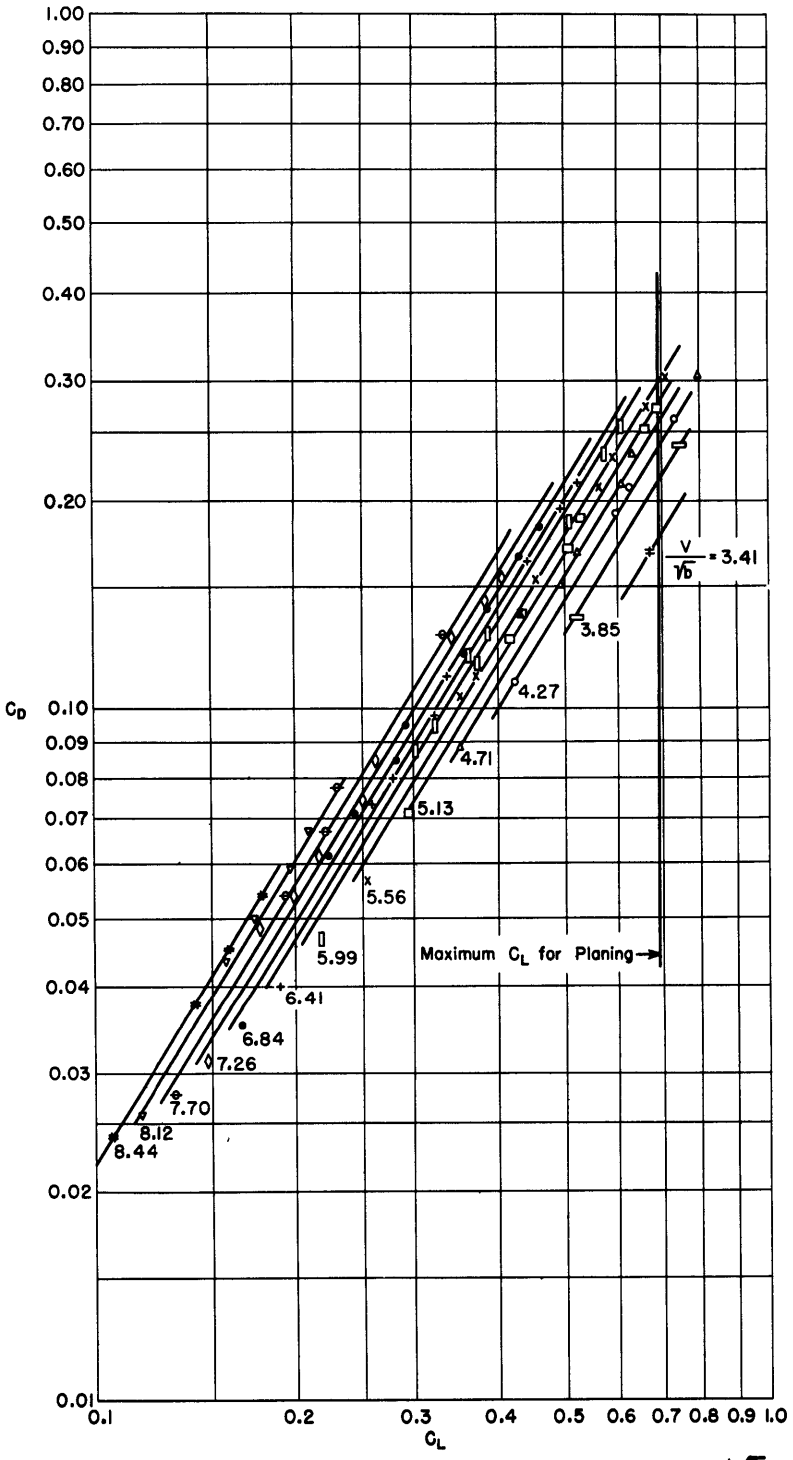

Figure 26 - Plot of C_D on C_L with Parameter $V/\sqrt{b}$ for the TMB Planing Float

$V/\sqrt{b}$. These data were compiled from all the values beyond the humps in Figure 10. Figure 26 shows that these values fall on a family of curves with a constant slope of 1.58 on the logarithmic plot, so that

$$\frac{C_D}{C_L^{1.58}} = f\left(\frac{V}{\sqrt{b}}\right) \qquad [11]$$

To check Equation [11], the original data were compiled in a plot of $\frac{C_D}{C_L^{1.58}}$ against $\frac{V}{\sqrt{b}}$ and, within the experimental error, were found to be represented closely by a single curve, Figure 27.

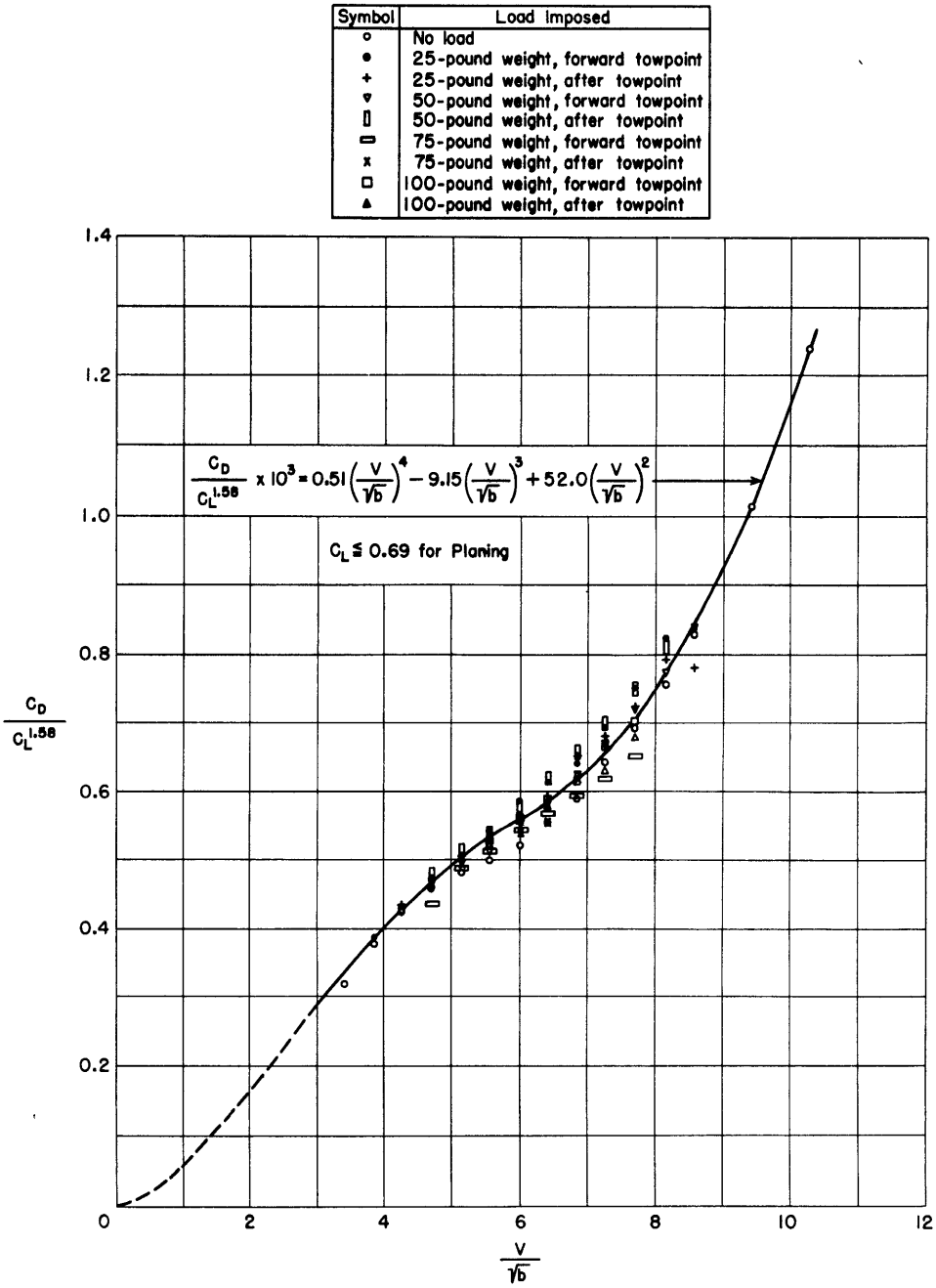

Figure 27 - Composite Plot of Data in the Planing Regime for the TMB Planing Float

The shape of the curve drawn through the data on Figure 27 was verified by comparison with a plot made on a similar basis of data available from tests under constant load of a number of high-speed planing boats. The mean curve through the data of Figure 27 can be closely approximated by the equation

$$\frac{C_D}{C_L^{1.58}} \times 10^3 = 0.51\left(\frac{V}{\sqrt{b}}\right)^4 - 9.15\left(\frac{V}{\sqrt{b}}\right)^3 + 52.0\left(\frac{V}{\sqrt{b}}\right)^2 \qquad [12]$$

when $C_L \leqq 0.69$.

In the actual design of a TMB float, therefore, the characteristics of a given float can be determined by first determining the regime in which the float will operate. This can be done by determining the value of C_L. If C_L is greater than 0.69, the methods of Reference (2) should be used. If C_L is equal to or less than 0.69, the characteristics can be determined from Figure 27 or Equation [12].

PERFORMANCE CHARACTERISTICS OF THE TMB DISPLACEMENT FLOAT

The development of the displacement float as an alternate to the planing float was dictated by a particular specification of the material to be used in its construction. Since the most practicable shape for a balsa-wood float was considered to be a body of revolution, the alternate float necessarily is of the displacement type.

Unlike the TMB planing float, which develops dynamic lift through planing action, the TMB displacement float derives its load-carrying capacity almost wholly from the hydrostatic forces on the float. As a result, the total load on this float should never be allowed to exceed its reserve buoyancy. The planing float, on the other hand, can carry loads which increase with towing speed provided that the dynamic lift on the float increases at least as fast as the imposed load.

Before presenting the techniques and results of the tests and the method finally used in the analysis of the displacement-float data, the design features of this float and the reasons for their selection are discussed.

DESIGN OF THE TMB DISPLACEMENT FLOAT

The displacement float designed for the catenary-sweep application was based on the design of the "O" type minesweeping float (9). However, the TMB float has a higher aspect ratio (or diameter-to-length ratio), which necessitates relatively larger tail surfaces than those on the "O" float in order to provide control area outside the wake of the hull.

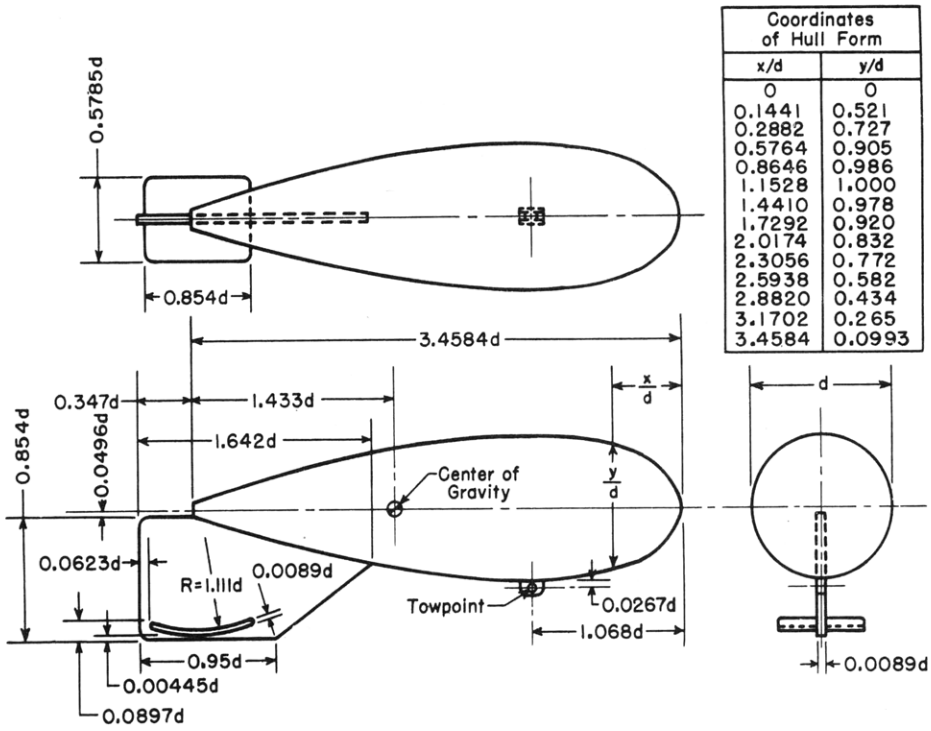

Coordinates of Hull Form	
x/d	y/d
0	0
0.1441	0.521
0.2882	0.727
0.5764	0.905
0.8646	0.986
1.1528	1.000
1.4410	0.978
1.7292	0.920
2.0174	0.832
2.3056	0.772
2.5938	0.582
2.8820	0.434
3.1702	0.265
3.4584	0.0993

Figure 28 - Dimensioned Sketch of TMB Displacement Float

All dimensions are referred to the maximum diameter *d*.

A drawing of the TMB displacement float in which all of the dimensions are referred to the maximum diameter is shown in Figure 28. A photograph of the test model is shown in Figure 29. This model was 48.6 inches long and 14.05 inches in diameter at its maximum diameter. The hull was constructed of balsa wood,* and all fittings were made of sheet brass. The model weighed 36 pounds and had a reserve buoyancy of 135 pounds.

The elevators providing downward lift at the stern were designed for two specific purposes. At low speeds, the pressure distribution around the hull produces a downward component of force which tends to make the float trim by the

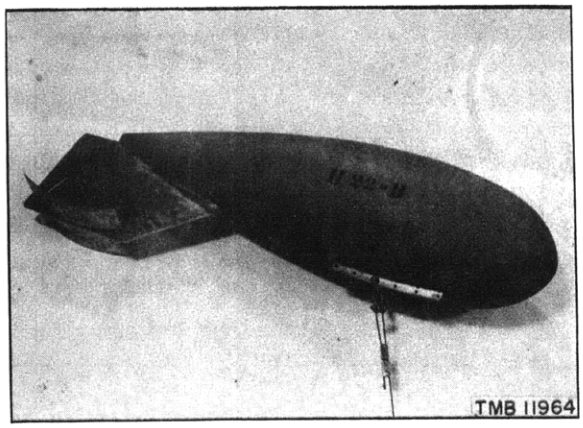

Figure 29 - TMB Displacement Float

This float is an experimental model showing the final positions of the elevators and the towpoint selected for optimum performance. The elevators are set at zero degrees. All dimensions and the position of the towpoint correspond to Figure 28.

* For a discussion of the methods of construction and waterproofing of the balsa-wood hull, see Appendix 4.

bow. The development of dynamic lift by the elevators largely offsets the downward force on the hull, so that the float remains on a more or less even keel. The combined effect, however, results in a greater submergence than would be obtained without the elevators. As the speed is increased, the increase in lift on the large elevators is sufficient to cause a positive increase in the angle of attack (or trim) of the float. As the angle of attack is increased, the hull, acting as a hydrofoil of very low aspect ratio, develops sufficient dynamic lift to cause the float to begin to rise. This sequence is illustrated by a number of photographs which were taken during the model-basin tests and which are discussed below.

TECHNIQUES AND RESULTS OF TESTS OF THE TMB DISPLACEMENT FLOAT

The same methods were used in the model-basin tests of the TMB displacement float as were used for the planing float. However, before systematic load-carrying tests were made with the displacement float, a number of tests under a single loading condition were first carried out to determine

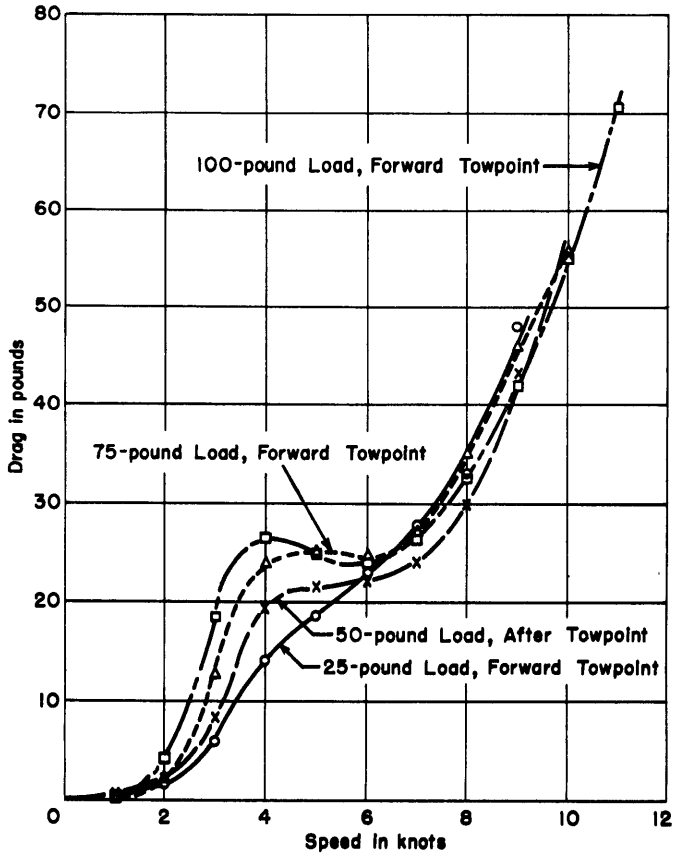

Figure 30 - Drag Curves for TMB Displacement Float

the best positions of towpoint and elevators. The tests were made under loads imposed by the 100-pound weight towed from the forward towpoint. The combination finally selected as giving the best performance is that shown in Figures 28 and 29.

Following the selection of the best elevator and towpoint positions, systematic towing tests under four loading conditions were carried out. The results of these tests are plotted in Figure 30. Photographs of the float taken during the model-basin tests are shown in Figures 31 through 34. The action of the float throughout the range of speeds at which tests were made is shown by these photographs. At low speeds, the float operated partly above the water surface under all imposed loads. As the speed was increased, the development of negative pressures produced a downward component of force on the float with ultimate complete submergence. With an increase in the angle of attack due to the increased lift on the elevators at the higher speeds, the float again approached the surface.

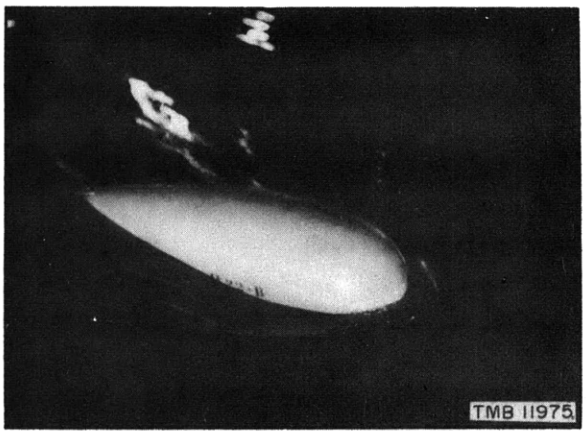

Towing Speed, 2.0 Knots

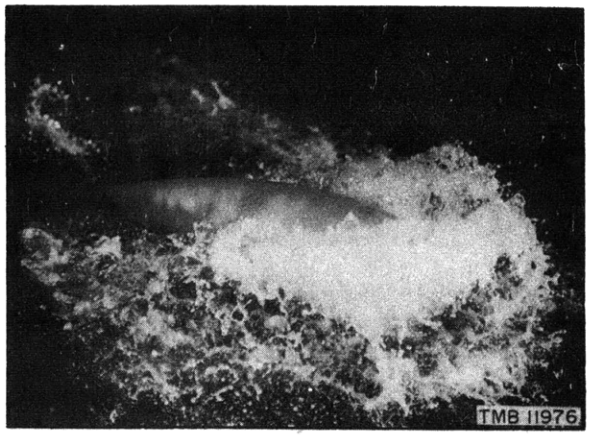

Towing Speed, 6.0 Knots

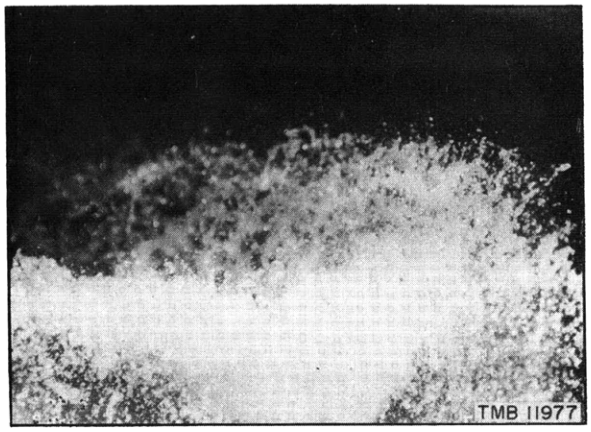

Towing Speed, 8.0 Knots

Figure 31 - Photographs of the TMB 48.6-Inch Displacement Float Being Towed

These tests were made under loads imposed by the 25-pound weight towed from the forward towpoint. The float did not become submerged under this set of conditions.

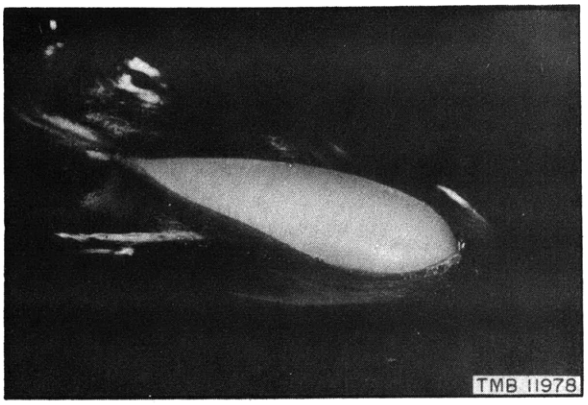

Towing Speed, 2.0 Knots

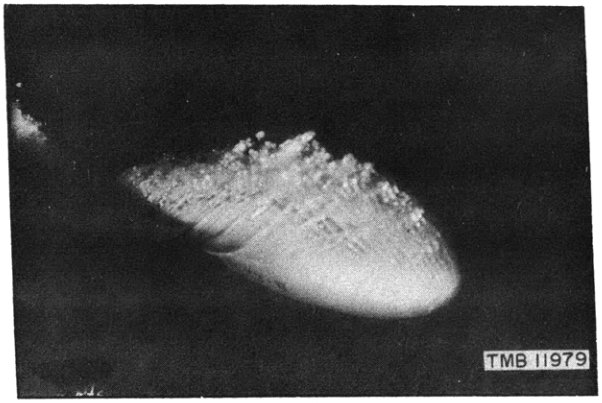

Towing Speed, 6.0 Knots

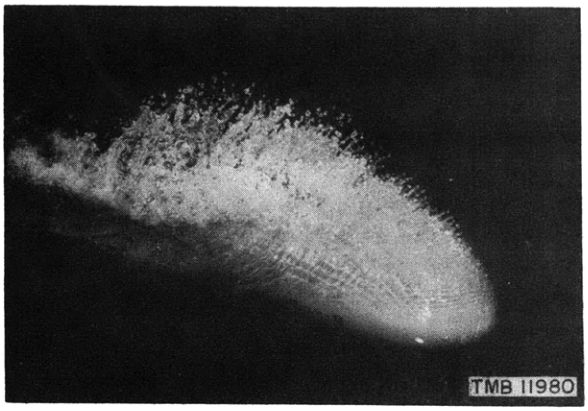

Towing Speed, 8.0 Knots

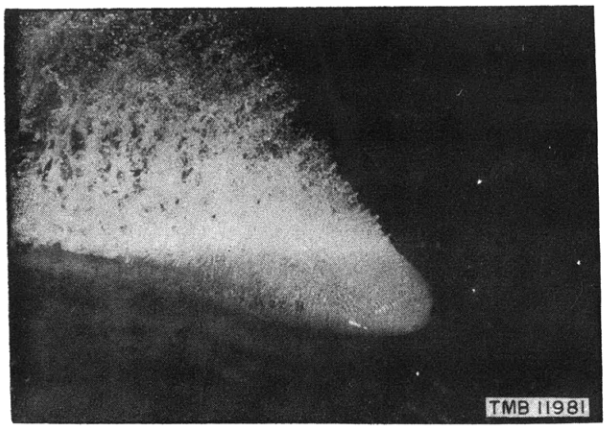

Towing Speed, 10.0 Knots

Figure 32 - Photographs of the TMB 48.6-Inch Displacement Float Being Towed

These tests were made under loads imposed by the 50-pound weight towed from the after towpoint.

The model towed stably up to the highest speeds shown on Figure 30 for each loading condition. Above these speeds there occurred an oscillatory instability in roll which appeared to increase with speed. This instability was observed to occur at the speed at which actual transition upward through the water surface (as defined for the TMB planing float in the foregoing) began. However, no attempts were made to investigate this phenomenon further, since the float, which had been designed for a specific purpose, performed satisfactorily under all loads throughout the speed range originally specified.

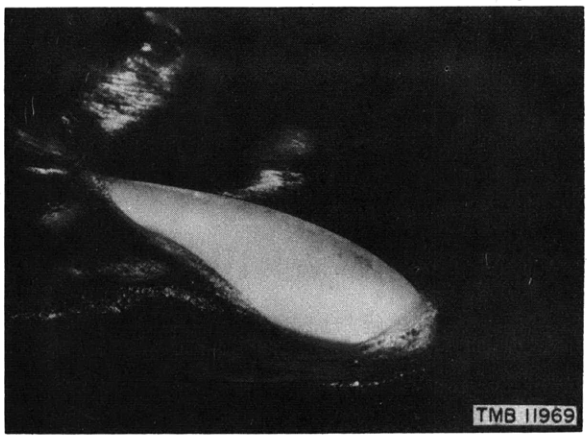

Towing Speed, 2.0 Knots

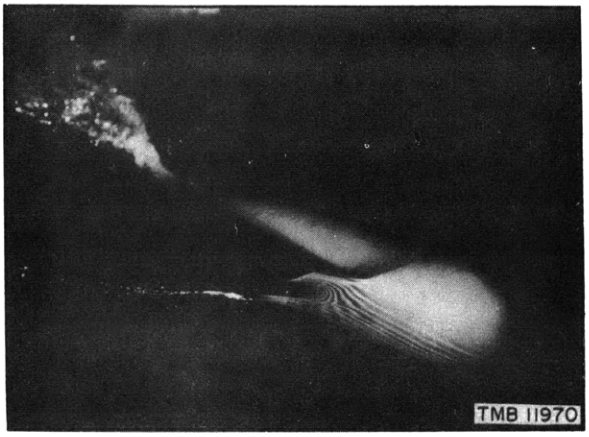

Towing Speed, 4.0 Knots

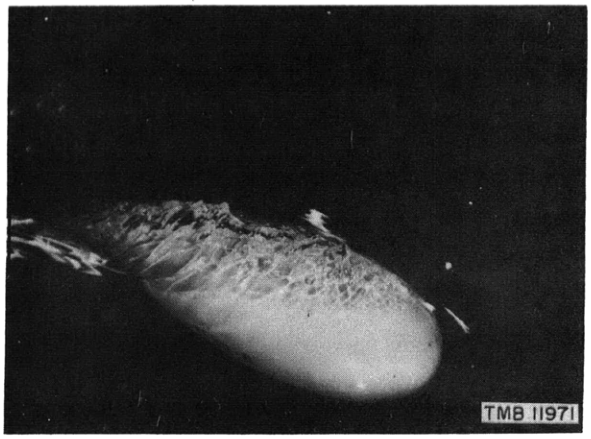

Towing Speed, 7.0 Knots

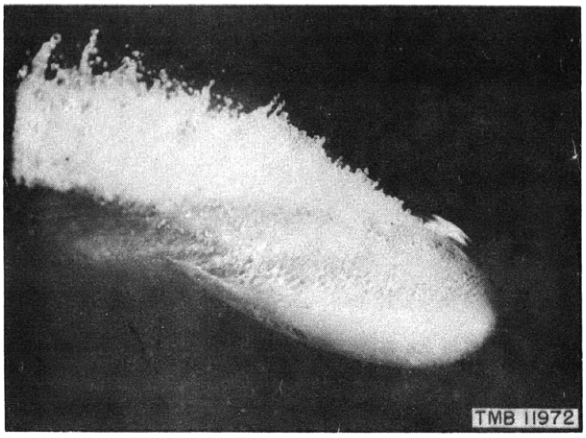

Towing Speed, 9.0 Knots

Figure 33 - Photographs of the TMB 48.6-Inch Displacement Float Being Towed

These tests were made under loads imposed by the 75-pound weight towed from the forward towpoint.

DISCUSSION AND ANALYSIS OF THE TMB DISPLACEMENT-FLOAT DATA

Turning now to the resistance of the float, the frictional drag is apparently a small percentage of the total drag for Reynolds numbers that are adequately large. The transition from laminar to turbulent boundary layer occurs at comparatively low Reynolds numbers for the type of form tested, about 5×10^5 to 2×10^6, as verified from comparison with ship model data as well as with a highly streamlined airship form (10). In general, the frictional drag coefficient for smooth streamlined bodies is small in turbulent flow and decreases with increasing Reynolds number; this condition holds for the float under discussion. Estimates of the frictional drag at the highest Reynolds number attained in the tests, 6.8×10^6, show that the frictional part of the drag is only of the order of 15 per cent of the total.

Towing Speed, 2.0 Knots

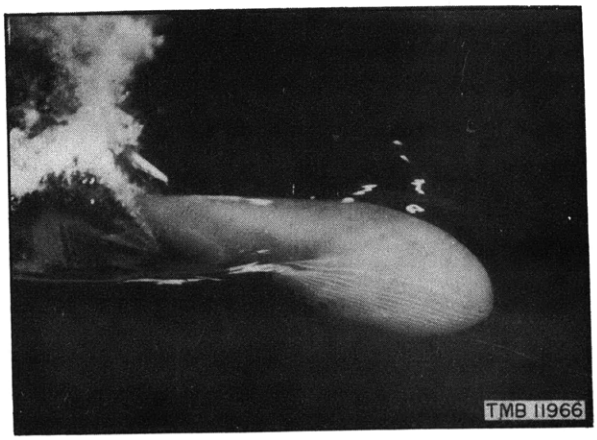

Towing Speed, 4.0 Knots

Towing Speed, 7.0 Knots

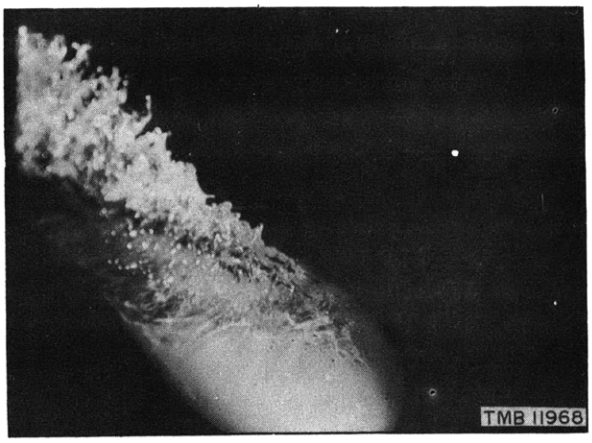

Towing Speed, 10.0 Knots

Figure 34 - Photographs of the TMB 48.6-Inch Displacement Float Being Towed

These tests were made under loads imposed by the 100-pound weight towed from the forward towpoint.

Hence, the total drag is chiefly composed of wave-making and form drag for the conditions under which the displacement float operates. For purposes of analysis, accordingly, the coefficients of total drag are assumed to have little dependence on the Reynolds number.

The humps in the curves of Figure 30 indicate the speeds at which the bow and stern waves are in phase, giving rise to large wave-making resistance. With an increase in speed beyond the humps in the curves of Figure 30, the resistance was actually found to decrease for the two higher loading conditions. This is due to the fact that the float under these conditions became sufficiently submerged so that wave-making resistance was greatly reduced, whereas the form or pressure drag and the frictional resistance continued to increase. For loads imposed by the 50-pound weight towed from the after

towpoint, the effect is less marked and an actual minimum does not occur in the drag curve. For the lightest loading condition, under which the float remained unsubmerged throughout the entire speed range, the drag curve shows the form characteristic of the resistance of surface vessels. At the higher speeds, the drag of the float is higher under the lightest loads than under heavier loads. This is a direct result of the fact that the float remained on the surface under this condition, whereas it did not return to surface operation under the other loadings. Comparison of the curves of Figure 30 with the photographs of Figures 31 through 34 shows clearly the correlation between the resistance curves and the performance of the float at the various speeds and loads.

In order to put these data into a form more useful for design purposes, it is possible to describe the drag of the float in terms of a nondimensional drag coefficient C_D as a function of a load or displacement coefficient C_Δ and the speed-length ratio $V/\sqrt{d}$. Since the coefficient of frictional resistance will remain roughly a constant over the range of Reynolds numbers in which this design is likely to be used, and for the reasons outlined above, dependence on Reynolds number may be neglected. As a result, the drag characteristics may be written in the functional relationship

$$C_D = C_D\left(C_\Delta, \frac{V}{\sqrt{d}}\right) \qquad [13]$$

where

$$C_D = \frac{D}{\frac{2.85}{2}\rho V^2 d^2} \qquad [14]$$

and

$$C_\Delta = \frac{\Delta}{w d^3} \qquad [15]$$

where D is the drag of the float in pounds,
ρ is the mass density of the fluid in slugs per cubic foot,
V is the speed in knots,
d is the maximum diameter of the float in feet,
w is the weight of the fluid in pounds per cubic foot, and
Δ is the total load on the float, including the weight of the float itself, in pounds.

The data of Figure 30 reduced to nondimensional form are shown in Figure 35 as a plot of C_D on a basis of $V/\sqrt{d}$, with C_Δ as a parameter. The values of the load coefficient represent means of the values actually derived from the loading conditions at each spot. The maximum deviation of the actual coefficient at each spot from the value shown on the corresponding curve

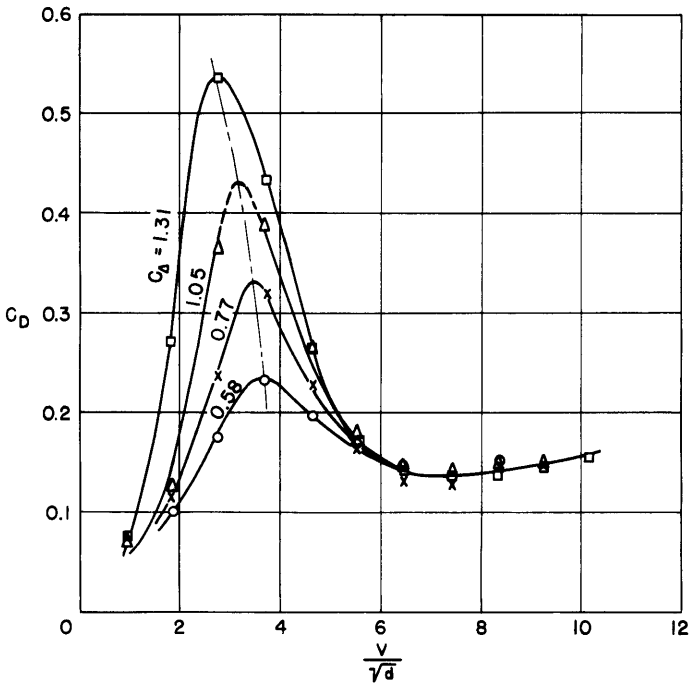

Figure 35 - Nondimensional Plot of Characteristics of TMB Displacement Float

was ± 3 per cent and thus within the experimental error; this justified drawing the family of curves shown in Figure 35.

The mode in which the resistance of the float changes is exhibited very clearly in Figure 35. The positions of the humps are clearly defined, and the rapid drop in drag coefficient as the float becomes submerged is sharply emphasized. That all the spots fair into a single curve beyond a speed-length ratio of about 6 indicates that the drag coefficient is very nearly independent of load at sufficiently high speeds. However, the drag coefficient for the parameter $C_\Delta = 0.58$ appears to rise above the curve at $\frac{V}{\sqrt{d}} = 8.3$, so that this conclusion may be valid only as long as the float remains at least slightly submerged.

COMMENTS ON THE USE OF THE TMB DISPLACEMENT-FLOAT DATA FOR DESIGN PURPOSES

TMB displacement-float data as presented in Figure 35 provide design criteria for most ranges of load and speed that are likely to be encountered. However, the present data are not extensive enough to derive an optimum float of this design for a given application, especially as regards stability, at speed-length ratios greater than those covered by the experiments described herein. Concerning the question of stability, it can be assumed that stable designs will result for all C_Δ and $\frac{V}{\sqrt{d}}$ within the range

of values shown on Figure 35 provided the float remains at least slightly submerged. This conclusion is based on the observation discussed in the foregoing that the float became unstable for $C_\Delta = 0.58$ at a speed-length ratio greater than 8.3. This is probably not a serious shortcoming, however, since most designs will involve greater loadings and the float will consequently become submerged.

The problem of an optimum design remains to be investigated, since the value of $C_\Delta = 1.31$ does not represent the maximum allowable load that may be imposed on the float. Since the float will develop increased lift with increased submergence, reaching a maximum value at some depth greater than that tested, the optimum value of C_Δ will be somewhat higher than 1.31. On the other hand, if the required performance is dictated by considerations of visibility, the value of 1.31 may well represent the optimum, especially if the float is to remain afloat when at rest under load. At any rate, for applications in which maximum loading is desired, e.g., small, efficient floats for supporting very deeply submerged loads, further calibration would be necessary.

CONCLUDING REMARKS

The analysis of the characteristics of the TMB planing float in the planing regime showed that the relation between total load, total drag, and speed-length ratio can be represented by a single equation. Although the method used in this analysis was checked on data available for several planing boats, it must be remembered that the analysis neglects any dependence on Reynolds number. It would appear doubtful that a unique relationship of the type derived can be obtained for large planing surfaces over a wide range of Reynolds numbers in which there is a large variation in frictional drag coefficients. It may be concluded, however, that the method may prove applicable to planing boats which are running in the planing regime but are heavily loaded, so that the pressure drag and the wave-making resistance will undoubtedly be much higher than the frictional drag. Here again, however, predictions of full-scale performance from model tests of planing boats analyzed in this way must be accepted with caution since the magnitude of the error involved in the assumptions, though not important for the range of floats likely to be used, cannot ordinarily be tolerated in the design of comparatively large boat hulls.

The foregoing remarks would also apply to a very large form similar to the TMB displacement float, although there do not appear to be any practical applications in water for such a form. It is clear, furthermore, that the type of analysis used for the displacement float, as well as the planing

float, succeeds only because the wave-making and form drags are the dominant contributions to the total drag.

With respect to the hysteresis loop discovered in the drag characteristics of the planing float in transition through the air-water interface, it was shown that there are two possible types of flow. The type in which water is thrown forward and to the sides was observed to be more stable than the other type in which the water continues to pass over the top of the float. The region near the speed at which transition begins is very unstable with the flow tending to oscillate between the two types. Finally, any disturbance of the flow of the second type causes a complete breakdown, and the flow goes over into the more stable type.

The phenomenon of striation formation requires further investigation. It may be possible to test experimentally the hypothesis concerning vortex instability by a series of high-speed photographs of a very smooth sphere dropped through an air-water interface. Such photographs would disclose any transverse oscillations that may occur if the vortex near separation does behave in the same manner as a free ring. It is doubtful that such tests could be made with a float because of the difficulty in holding the float for any length of time in the type of flow in which these striations occur. It would be desirable to have the sphere highly polished to minimize the formation of cavities about irregularities on the surface of the specimen. At the present time, however, this phenomenon appears to be only of academic interest. If it were found that such formations are detrimental, e.g., in terms of drag, the practical problem presented would probably be one of boundary-layer control.

REFERENCES

(1) BuShips CONFIDENTIAL letter C-S81-1(3)(620) of 7 September 1943 to TMB.

(2) "Design and Performance of the TMB Planing Float as a Towed Position Indicator," by L. Landweber and Ensign P. Eisenberg, USNR, TMB Report 540, March 1945.

(3) TMB CONFIDENTIAL letter C-S81-1 of 6 March 1944 to BuShips, Minesweeping (620).

(4) "Characteristics of Clark Y Airfoils of Small Aspect Ratios," by C.H. Zimmerman, NACA Report 431, May 5, 1932.

(5) "Characteristics of the NRL Mark 3 Boat-Type Buoy and Determination of Mooring-Line Sizes," by Ensign P. Eisenberg, USNR, TMB Report 550, September 1945.

(6) "Preliminary Tests in the NACA Tank to Investigate the Fundamental Characteristics of Hydrofoils," by Kenneth E. Ward and Norman S. Land, NACA ACR, September 1940.

(7) "Modern Developments in Fluid Dynamics," edited by S. Goldstein, Vol. 1, Oxford University Press, 1938.

(8) "Über eine experimentell beobachtete Erscheinung an Wirbelringen bei ihrer translatorischen Bewegung in wirklichen Flüssigkeiten" (On Experimentally Observed Phenomena on Vortex Rings and Their Translatory Motion in Ordinary Liquids), by Carl-Heinz Krutzsch, Annalen der Physik, Vol. 35, Series 5, 1939.

(9) Bureau of Ships plan 455432, "O" Type Mine Sweep Size No. 4 - Arrangement and Details of Mark 3 Float, dated 21 June 1941.

(10) "Measurements of Flow in the Boundary Layer of a 1/40-Scale Model of the U.S. Airship AKRON," by Hugh B. Freeman, NACA Report 430, April 27, 1932.

(11) "Progress Report on the Lateral Vibrations of Circular Cylinders Caused by Motion Through a Fluid," by L. Landweber and G. Grimminger, TMB File C-SS/S24-9, January 1940.

The following reports were prepared by the Industrial Test Laboratory, Navy Yard, Philadelphia, Pa., on tests of various waterproofing and fireproofing materials for balsa-wood life rafts:

(12) "Proposed Tests of Floats for Buoyant Life Nets," ITL Report 1410, 30 September 1943.

(13) "Test of Balsa Life Raft Coating for Balsa Wood Life Rafts," ITL Report 1220-B, 12 January 1943.

(14) "Buoyant Life Net Floats," ITL Report 1610, 5 October 1943.

(15) "Synthetic Plasoleum Covered Balsa Life Floats," ITL Report 1639, 28 August 1943.

(16) "Proposed Balsa Wood Alternate for Floater Net Floats," ITL Report 1510, 29 July 1943.

(17) "Proposed Natural Plasoleum Cement Coating for Life Floats," ITL Report 1456, 17 December 1943.

(18) "Balsa Wood Life Floats: Test of Alternate Methods of Covering," ITL Report 1220-C, 21 May 1943.

(19) "Floater Net Floats Treated With Eclut," ITL Report 1580, 29 November 1943.

(20) "Neoprene Cement Coating for Balsa Wood Life Floats," ITL Report 1216-B, 25 October 1943.

APPENDIX 1

TESTS OF THE NAVAL MINE WARFARE TEST STATION FLOAT

DESCRIPTION OF THE NMWTS FLOAT

The NMWTS float, Figure 36, was evidently designed originally as a static marker buoy without thought to its subsequent application as a towed float. It appears, therefore, that its use for towing was suggested on the basis of simplicity of construction and ease of handling. The model submitted for test was of hollow sheet-metal construction and weighed approximately 27 pounds with a total buoyancy of 130 pounds in sea water. The float hull has no auxiliary surfaces for either lift or stabilization.

It was requested that tests be made with two methods of towing. The first was to tow from a point on the hull 4 inches forward of the center

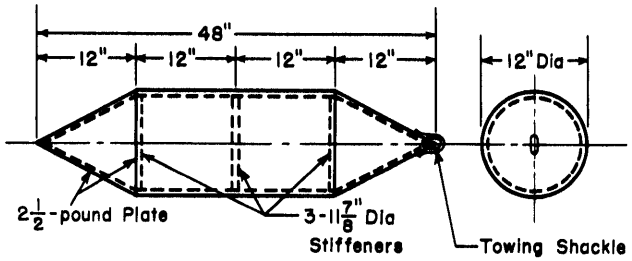

Figure 36 - Float for Catenary Sweep Submitted for Test by Naval Mine Warfare Test Station

stiffener. This method immediately proved impracticable since the float turned broadside to the stream and was entirely unstable. As a result, systematic tests were made only with the float towed from a shackle welded to the nose as shown in Figure 36.

RESULTS OF THE NMWTS FLOAT TESTS

Towing tests were conducted under four conditions of load in the manner described in the body of this report. The drag of the float under the loading conditions corresponding to the curves of Figure 8 is shown in Figure 37. Photographs of the float taken during the tests are shown in Figure 38.

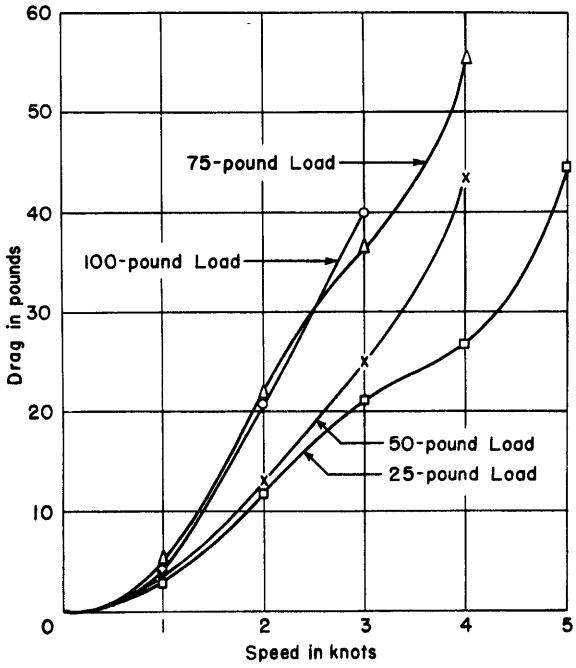

Figure 37 - Drag of NMWTS Float under Various Loading Conditions and Towed from the Forward Towpoint

Since at low speeds the float is essentially a cylinder towed transversely to the stream, the flow is such as to produce a Kármán vortex street in which eddies are shed alternately from either side of the float. The periodic shedding of eddies gives rise to alternating side forces with the result that the float is oscillated with the frequency of the eddy wake (11). The oscillation of the float is indicated to some extent in the photographs of Figure 38 in which the angle made by the float with the vertical in the plane transverse to the flow is obvious.

As a result of the lateral oscillations of the float, the drag shows a cyclic variation about the mean. The results plotted in Figure 37 represent the mean drag as measured on the towing dynamometer, which was operated with a high degree of damping.

Owing to the high drag of this float and the fact that it rapidly loses lifting capacity because of its negative angle of attack or trim, its usefulness as a towed float is limited to very low speeds. Under the highest loading conditions used in the tests, the float was considered completely overloaded above 3 knots. In view of these conclusions, this type of float is not recommended for towing operations. Furthermore, its use as a moored buoy should be limited to regions in which currents are small.

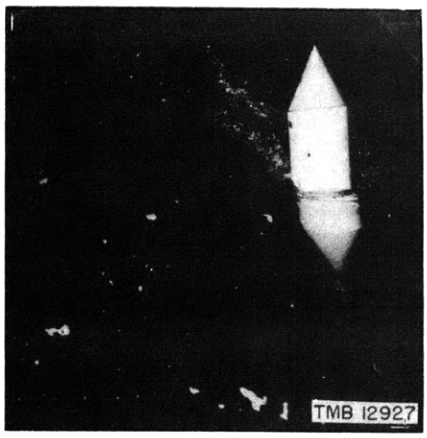

Towing Speed, 2.0 Knots

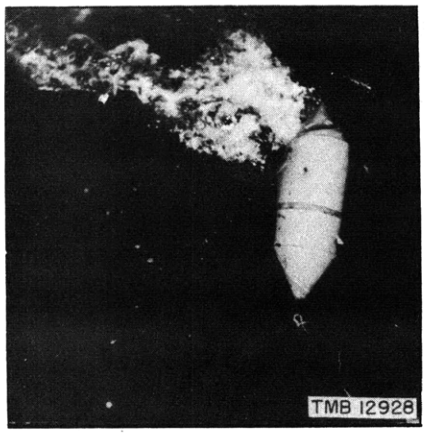

Towing Speed, 4.0 Knots

Figure 38a - Tests under Loads Imposed by 25-Pound Weight Towed from Forward Towpoint

Towing Speed, 2.0 Knots

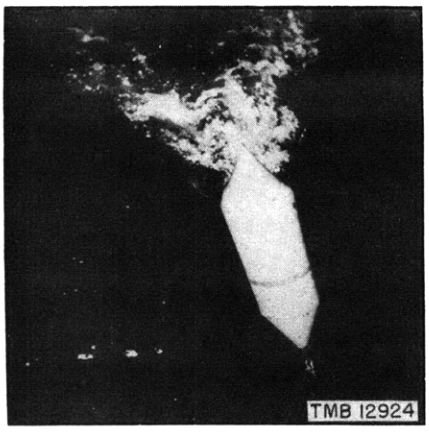

Towing Speed, 4.0 Knots

Figure 38b - Tests under Loads Imposed by 50-Pound Weight Towed from Forward Towpoint

Towing Speed, 1.0 Knot

Figure 38c - Tests under Loads Imposed by 75-Pound Weight Towed from Forward Towpoint

Figure 38 - Photographs of the NMWTS Float Being Towed

APPENDIX 2

TMB PLANING FLOAT AND NMWTS FLOAT APPLIED TO A CATENARY MINESWEEPING ARRANGEMENT

ORIGINAL SPECIFICATIONS

The original specifications for the catenary minesweeping project were based on the problem of towing a symmetrical loop of aluminum cable, 1800 feet long and 1.75 inch in diameter, weighing about 1.4 pound per foot in air and having a negative buoyancy of 0.55 pound per foot in sea water. Required towing speeds varied from 2 to 9 knots with the two ships on parallel courses and 330 yards apart. The maximum working tension of the cable was 6000 pounds.

To avoid touching the bottom at low speeds in shallow water, it was desired to support the loop by floats attached at intervals along its length. At the lowest speed of 2 knots, it was required that the floats be designed so that the maximum depth of the cable would not exceed 30 feet. At no speed, however, was the depth to be less than 5 feet. If a float small enough to be handled manually was found to be adequate, its weight was not to exceed 75 pounds. If a larger float to be handled by a crane was required, its weight was not to exceed 200 pounds.

The first design based on these specifications was the TMB planing float described in the body of the report. With a sweep cable weighing 0.55 pound per foot in water, enough floats were required to carry a load of about 990 pounds at the minimum speed of 2 knots. Although the TMB planing float is designed to develop dynamic lift in addition to its reserve buoyancy at sufficiently high speeds, the minimum float size was based on the reserve-buoyancy requirements for the lowest specified towing speed. These conditions resulted in a preliminary design utilizing eleven TMB planing floats. The towing arrangement under these conditions is shown in Figure 1; the floats are secured to the nonbuoyant cable, and the two free tails are buoyant.

As outlined in the body of the report, the balsa-wood displacement float was subsequently designed for this project on the basis of a saving in weight. The NMWTS float was submitted for test on the basis of simplicity of construction.

Full-scale trials of the TMB planing float were scheduled before a request for the balsa-wood float had been received. For these trials, twenty planing floats were fabricated in the Taylor Model Basin shops. However, a much heavier cable was used during the trials than the aluminum cable originally specified. This necessitated the use of several NMWTS floats, which

gave an opportunity to observe the performance of these floats as well. These trials are described in the following section.

PROCEDURE IN FULL-SCALE SWEEPING OPERATIONS

Full-scale observations of the performance of the TMB planing float and of the NMWTS float were made on 11 March 1944 at the U.S. Naval Mine Warfare Test Station, Solomons, Maryland. In these tests twenty planing floats were used in conjunction with seven cylindrical floats on a single cable.

Although the original specifications called for the use of 1800 feet of aluminum cable having a negative buoyancy of 0.55 pound per foot, the trials discussed herein were made with 2000 feet of copper cable weighing 0.83 pound per foot in water. With a spacing of 75 feet between floats, each float was carrying approximately 63 pounds.

The arrangement used in the full-scale tests is shown schematically in Figure 39. Runs were made with the two identical towing ships separated

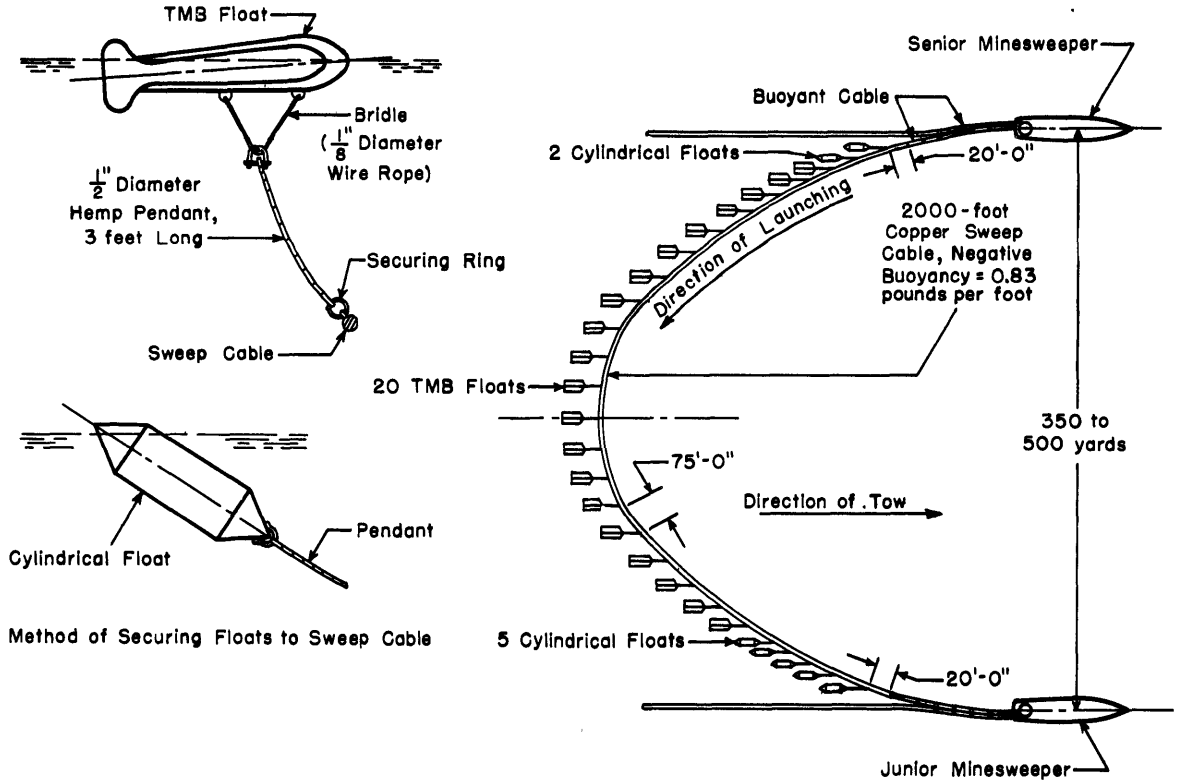

Figure 39 - Catenary-Type Sweep Towing Arrangement for Tests of 11 March 1944

by 350, 400, 450, and 500 yards. Observations were made at speeds up to 5.25 knots. Ship separation was measured by a stadimeter, and speeds were computed from taffrail-log readings. The total tension in the catenary-sweep cable and

in the buoyant cable was recorded with a dynamometer inserted in the line at each ship. At the highest towing speed the tension was approximately 5500 pounds.

Launching of the gear was accomplished from the senior minesweeper. The junior ship was brought alongside, and a line was passed from the senior vessel to establish the loop. The buoyant cables were then independently launched from each vessel. On the senior ship, the nonbuoyant cable and the buoyant cables were launched simultaneously from a single reel on the fantail. As the sweep cable was paid out, the floats were secured with a snap hook to a ring wired to the cable.

Although the specified depth of the nonbuoyant cable was 5 feet or greater but not in excess of 30 feet, a pendant only 3 feet long was used. The pendant was of hemp rope with swivels and eyes at each end. This short length was used because, in earlier trials with the copper cable in which twenty-one NMWTS floats were used, the tow became submerged and it was found, on retrieving, that the cable had been dragging on the river bottom. The observations made during the model-basin tests of the NMWTS float, Appendix 1, indicated that such an effect could be expected if only the cylindrical floats were used.

The method of securing the pendant to the floats is shown in Figure 39. For the TMB float the pendant was fastened to a shackle at the apex of the bridle, while on the cylindrical floats the pendant was made fast in a shackle welded to the apex of the cone.

OBSERVATIONS MADE DURING THE FULL-SCALE TRIALS

During the launching operations, one TMB float became fouled over the free buoyant cable in the manner shown in Figure 40. It appeared that the cylindrical floats were not as susceptible to fouling because of their shape and method of towing from the nose. From Figure 40, it is apparent that the cylindrical float requires less towline tension than the TMB float in order to free itself from the buoyant cable. However, as the catenary loop developed, the TMB float was pulled free of the buoyant cable and no further difficulties were encountered. For this particular project, it is believed that fouling can be prevented by careful launching. If the buoyant cable does wash over the top of the floats in a heavy sea or in cross currents, it can be freed by momentarily increasing the speed. By increasing the towing speed, the components of tension in the loop transverse to the direction of tow and the drag on the buoyant cable can be increased sufficiently to pull the fouled float under the buoyant cable and free that cable.

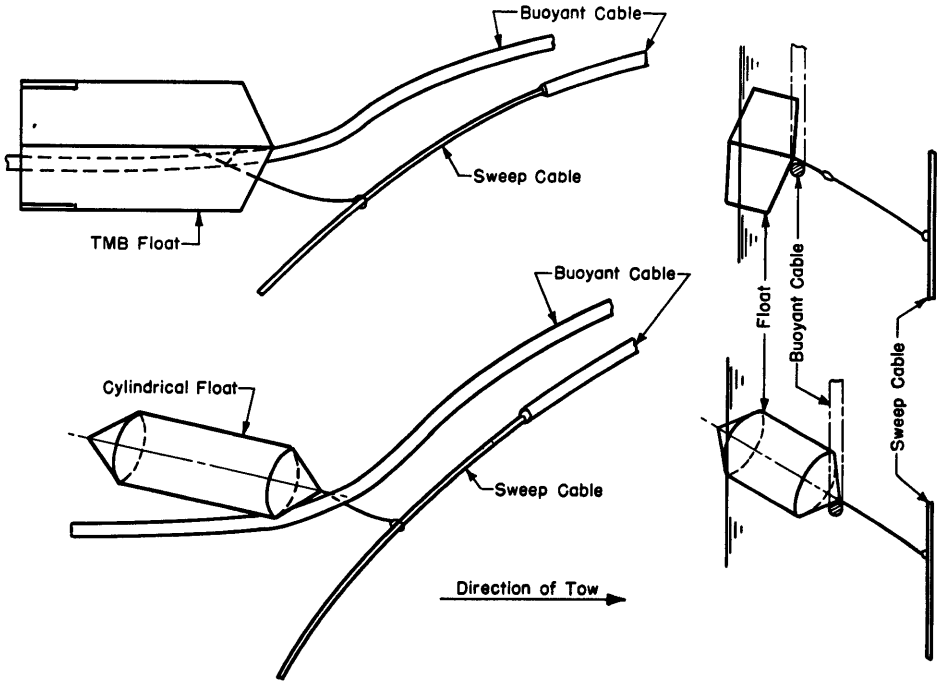

Figure 40 - Fouling of Buoyant Cable and Floats

Throughout the speed range up to about 4.5 knots, all floats towed submerged. The TMB floats were observed to be about 4 inches below the water surface. Above 4.5 knots, the TMB floats were closer to the surface and, at the highest speed of 5.25 knots, were towing on the surface. By interpolation on either Figure 10 or Figure 25, with an allowance for a slight decrease in load on the float due to the lift forces on the cable loop, it can be seen that the speed of "planing" observed during the field tests checks the model-basin observations. The seven cylindrical floats remained submerged throughout the day's testing. During the tests at high speed, it was possible to take observations of the shape of the loop by sighting on the TMB floats, all of which were visible. Such observations were not possible with the NMWTS floats, which remained submerged for reasons already discussed.

APPENDIX 3

SUBMERGENCE PRESSURE TESTS ON THE TMB PLANING FLOAT

PURPOSE AND SCOPE OF THE TESTS

Subsequent to the tests of the hydrodynamic properties of the TMB planing float, it was requested that external pressure tests be made in order to determine the maximum depth of submergence that the hollow metal float could withstand without collapse.

The submergence tests were made in the decompression chamber of the Naval Gun Factory, Washington, D.C. A sketch of the model used in these tests is shown in Figure 41. The float was airtight when introduced into the de-

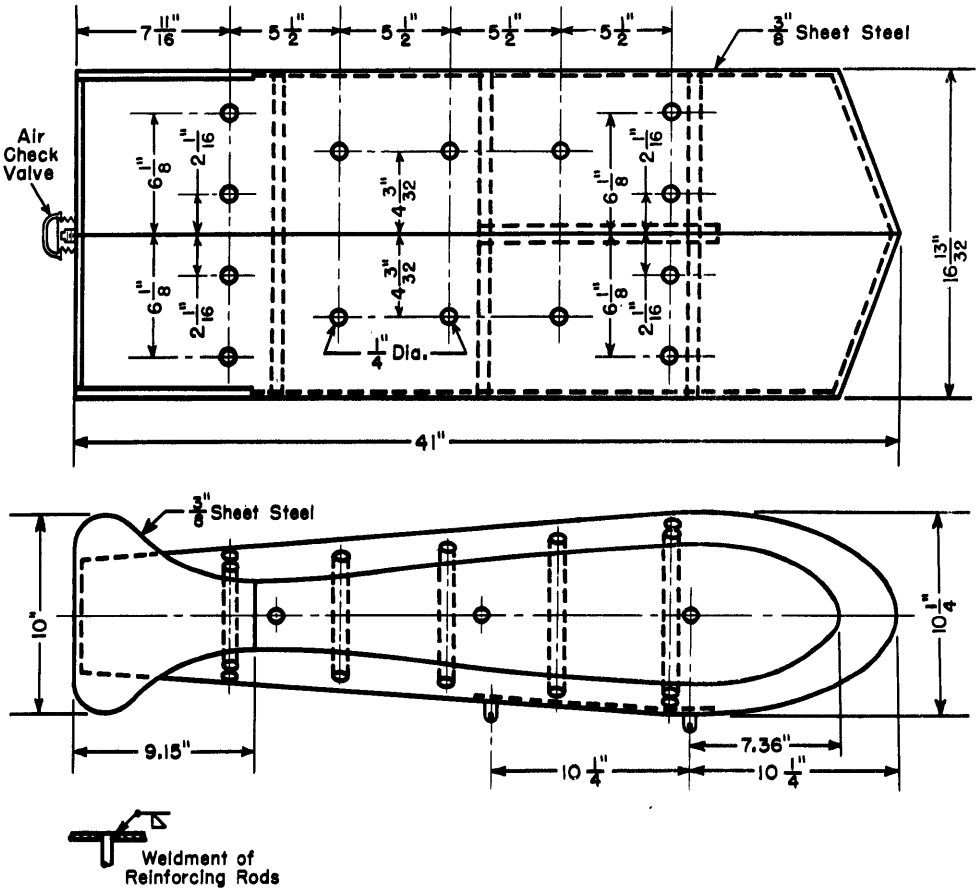

Figure 41 - Principal Dimensions of TMB 41-Inch Planing Float

compression chamber. The vertical and transverse rods are introduced only as simple tension members to reinforce the float against the prestressing pressure of 8 pounds per square inch, corresponding to 18 feet of sea water. During the pressure tests, however, no initial internal pressure was applied.

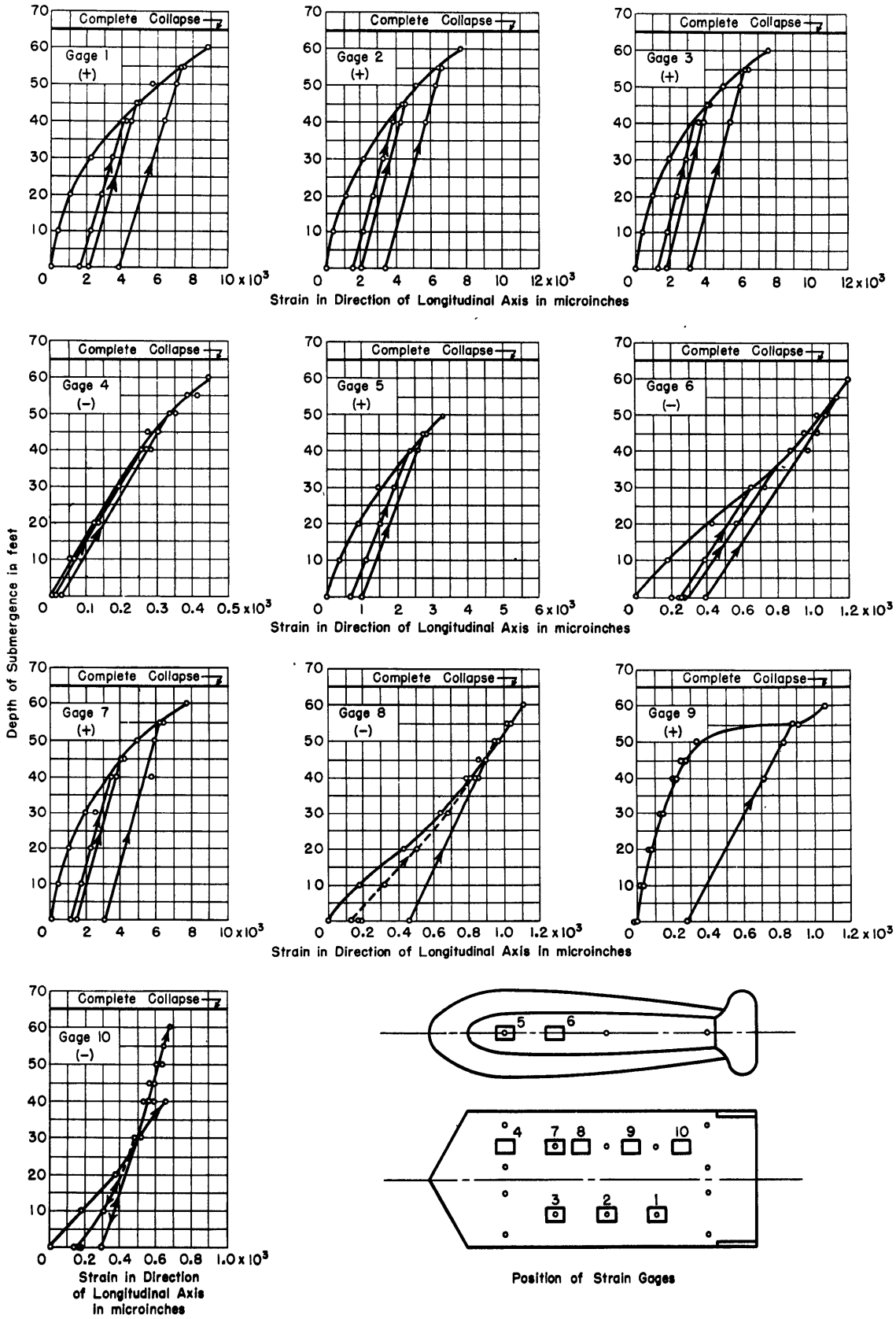

Figure 42 - Submergence Test of TMB Planing Float

Although it was intended merely to determine the maximum allowable depth of submergence, strain measurements were made at several points on the skin of the float in order to provide a somewhat clearer picture of the manner in which failure eventually occurred. These measurements were also intended to determine to some extent the permanent strain that could be allowed before the hydrodynamic properties were affected. However, up to the point at which the welds at the reinforcing rods failed, no deflections were visible in the skin that might have affected the hydrodynamic performance.

Resistance-wire strain gages were cemented to the skin of the float either directly over the ends of the reinforcing rods or at positions halfway between adjacent reinforcing rods, Figures 41 and 42. Since these tests were not intended to provide data for a complete analysis of the stresses in the float, the gages were arranged to measure only the longitudinal strains which were adopted as criteria of the allowable permanent set.

RESULTS OF THE SUBMERGENCE TESTS

The data obtained during the submergence tests of the planing float are shown in Figure 42 as curves of strain in microinches at various depths of submergence in sea water. The tests were stopped at three different depths, and the pressure was returned to atmospheric in order to observe the permanent set of the material. The signs adjacent to each set of curves indicate the direction of the strain, plus being used for tension and minus for compression. Although some extremely high strains were recorded, the associated deflections of the surfaces did not appear to be so excessive as to warrant additional tests of performance since any differences would be within the experimental error of the hydrodynamical characteristics discussed in the body of this report. Complete failure occurred at an external pressure corresponding to 65 feet of sea water, at which pressure the reinforcing-rod welds failed in the top surface and allowed collapse of the upper and lower surfaces. Photographs of the float taken shortly after completion of these tests are shown in Figure 43.

Although the design of the float was based on a maximum depth of submergence of 40 feet of sea water, using "black iron" with a yield point of 30,000 pounds per square inch, the results show that the steel actually used had a much lower yield point. The actual yield point of the material appears to have been approximately 10,000 pounds per square inch, indicating that a much poorer grade of steel had been inadvertently used than originally specified. Nevertheless, the present design is apparently controlled by the weldment of the reinforcing rods. It was originally proposed that the ends of

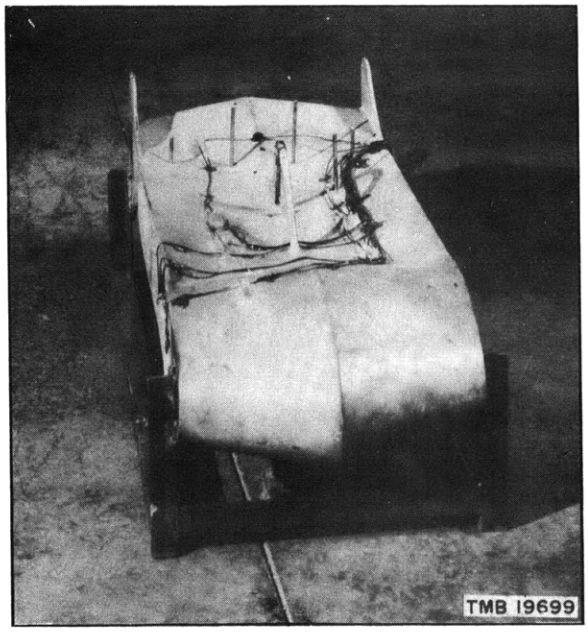

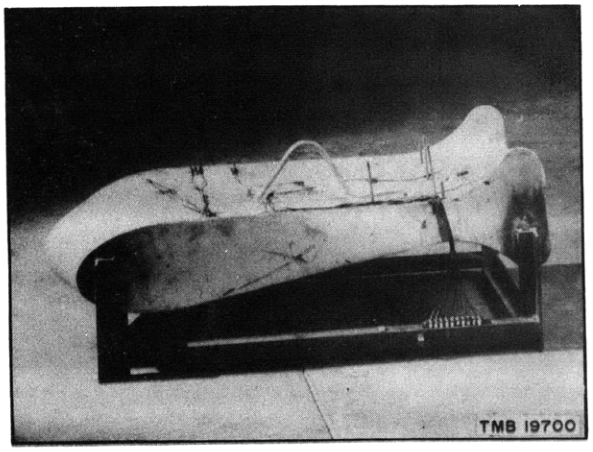

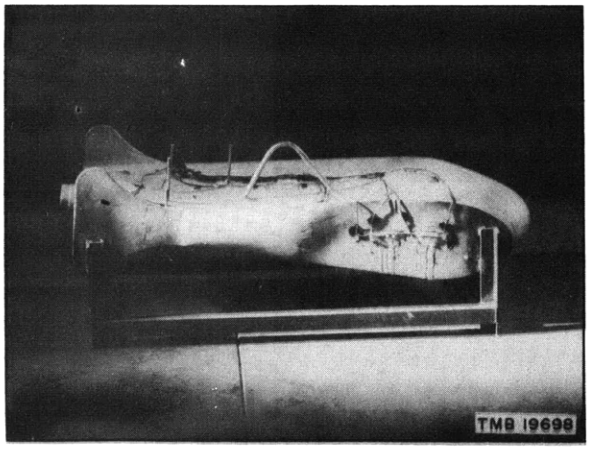

Figure 43 - Photographs of the TMB 41-Inch Planing Float after Submergence Tests

The reinforcing-rod welds have failed in the top surface of the float, and the rods have been pushed through. The flat surfaces have failed completely, while the curved surfaces at the bow do not show excessive deflections.

the rods be reinforced with small bushings to provide greater welding area. However, the additional cost did not warrant this step for the surface floats.

Based on these tests and the design used herein, and assuming that failure will occur in the welds, as it did on this float, a safe maximum depth of submergence can be assumed to be 75 feet of sea water, provided that an internal prestressing pressure of 8 pounds per square inch is used. A searching analysis of the strain data for purposes of providing design criteria is not warranted, however, because of the lack of essential measurements.

APPENDIX 4

NOTES ON THE CONSTRUCTION OF THE BALSA-WOOD FLOAT

PROCEDURE IN CONSTRUCTION OF BALSA-WOOD FLOAT

The method used in the construction of the balsa-wood float is included herein since the procedure was specifically developed for the pilot model and was subsequently used in the actual production of a number of these floats.

The method of preparing the balsa-wood form for turning the hull on a lathe is shown in Figure 44. The form was built up with laminations of

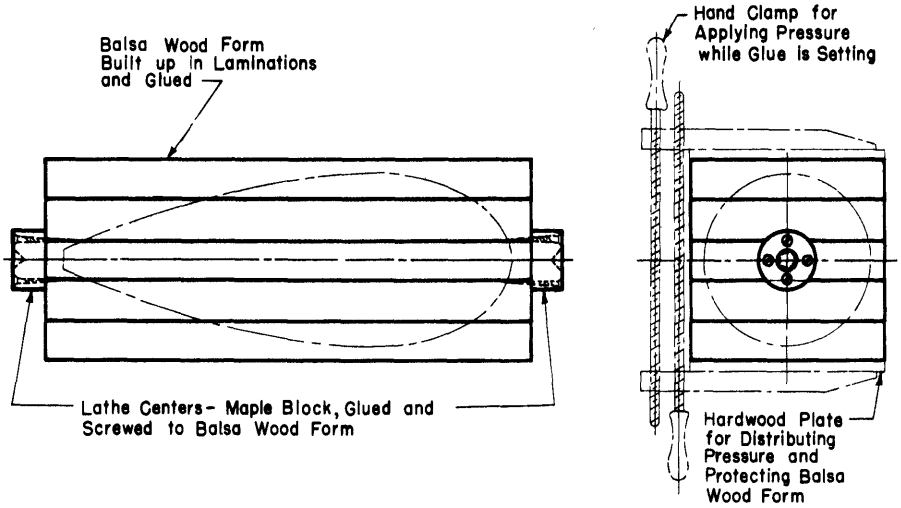

Figure 44 - Method of Preparing Balsa-Wood Form for Turning Float

balsa wood glued together. Both sides of each lamina were coated with one coat of "Weldwood" glue, a commercial plastic resin. The glue was allowed to dry under pressure applied with hand clamps in the manner illustrated in Figure 44. The clamps were tightened by hand alone. The ends of this form were then saturated with glue, and the maple-wood cylinders were glued and screwed to the form to serve as lathe centers. The form was then turned to the hull form. Spruce inserts for the towing bracket and the slot for the tail fin were added after the hull had been finished. The slot for the tail fin was filled with a waterproofing compound, commercially known as Eclut, and the tail fin was inserted before drying. A coat of Eclut was also applied to the spruce insert before adding the towing bracket.

Eclut was applied to the hull following the procedure recommended by the manufacturer. The first coat was allowed to dry for 24 hours, and subsequent coats were applied at 2-hour intervals. The first six coats were

brushed on to assure adherence to the wood, and the final three coats were sprayed on to supply a uniform finish. It is believed that brushing resulted in better adherence to the wooden hull than dipping in the compound.

NOTES ON THE USE OF BALSA WOOD AS A FLOAT MATERIAL

Although the use of balsa wood enabled a comparatively light-weight float to be constructed, the many disadvantages of the material do not recommend its use for an efficient load-carrying device. The extreme vulnerability to damage during launching and retrieving operations complicates the initial waterproofing problem as well as subsequent maintenance. Although the Eclut compound forms a fairly good coating on first application, it does not have adequate adherence properties, so that a small break in the skin aggravates the tendency to peel off as a solid sheet. Furthermore, a small break occurring during the launching operations immediately provides a point where absorption of water by the float can begin. The high porosity of balsa wood then results in early water-logging with subsequent loss in buoyancy and incipient decay.

Another difficulty lies in maintaining specifications of balsa-wood density among different manufacturers. Samples of balsa submitted for examination showed variations in weight as high as 70 per cent. As a result, it becomes necessary to specify moisture contents and seasoning procedure, which leads to higher costs in manufacture.

For discussions of the properties of Eclut as well as other waterproofing compounds and materials, References (12) through (20) have been listed. These papers report results of adhesion, breaking, dropping, and fireproofing tests of various materials.